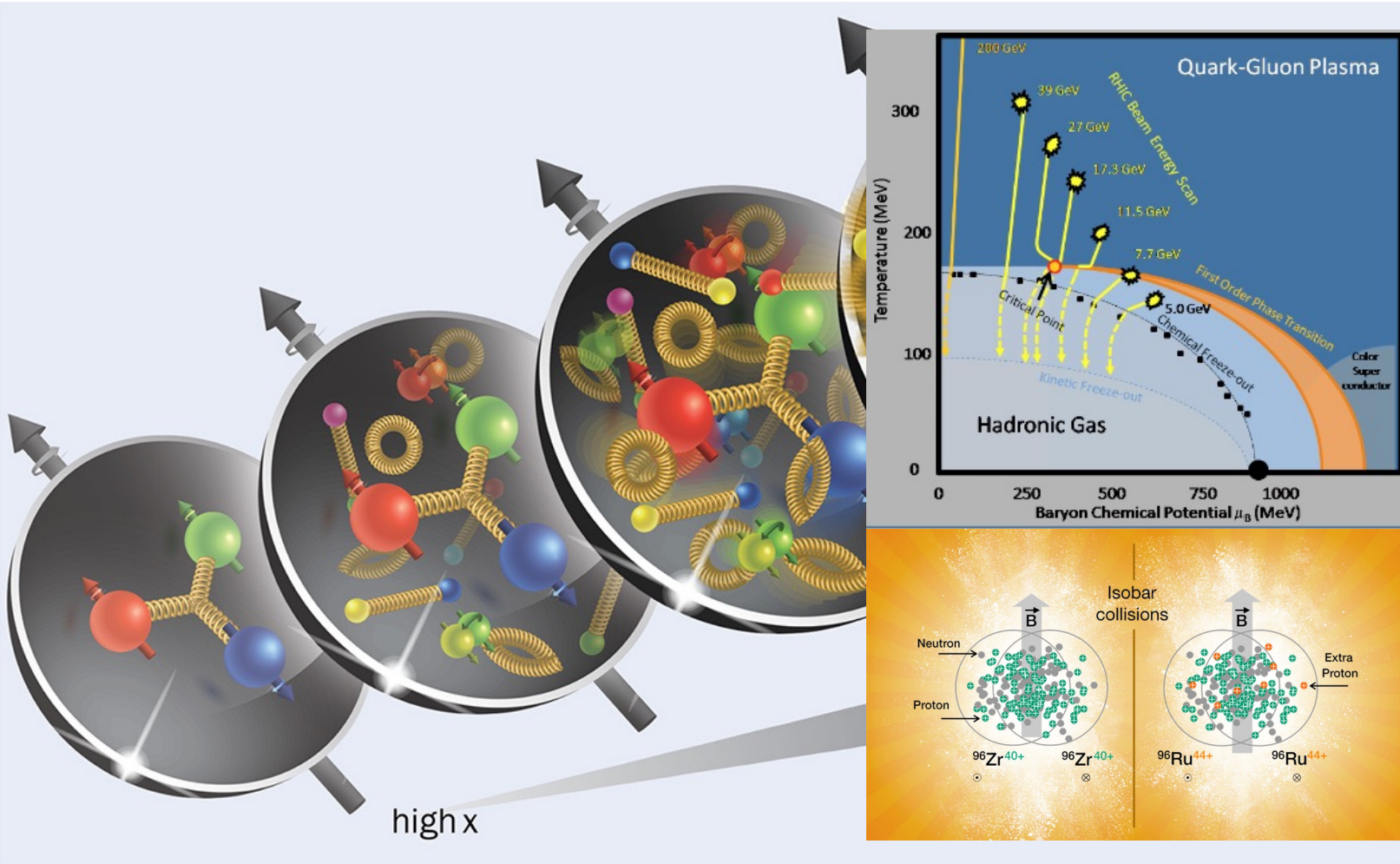


# STAR toward EIC

Zhangbu Xu



[https://indico.bnl.gov/event/20331/contributions/79937/attachments/49634/84868/BUR2024to25\\_STAR.pdf](https://indico.bnl.gov/event/20331/contributions/79937/attachments/49634/84868/BUR2024to25_STAR.pdf)

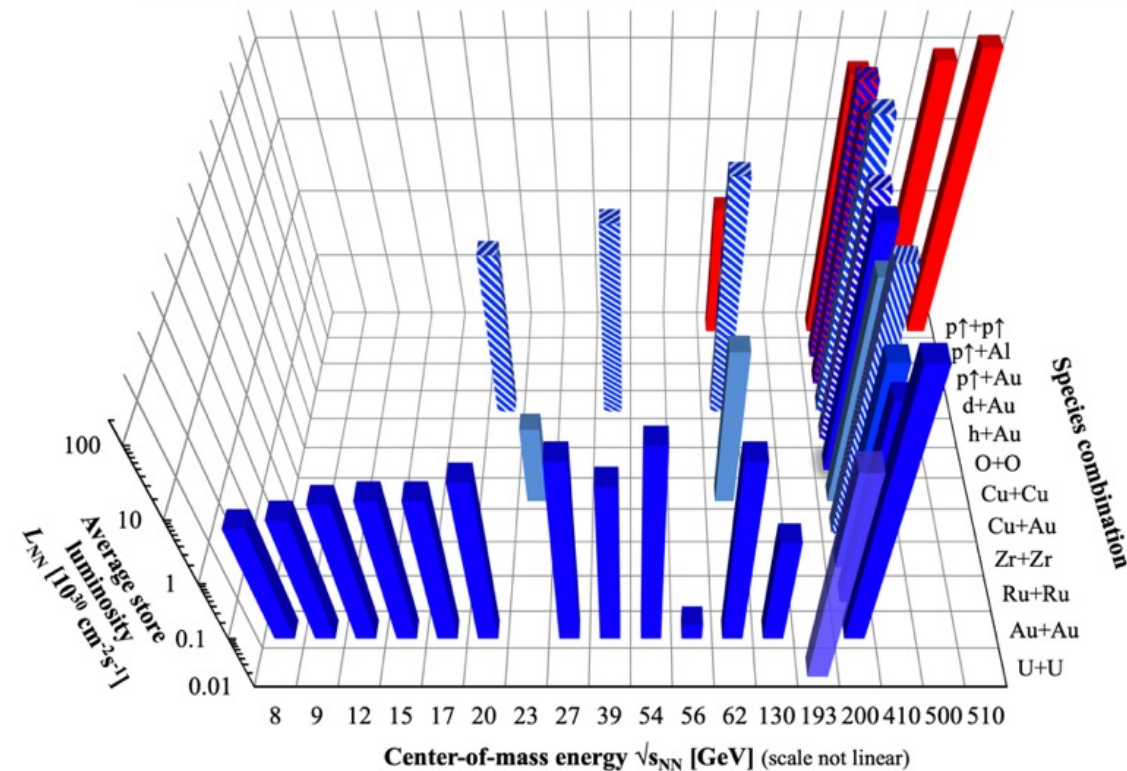
EIC-Asia Workshop, 01/29/2024



# Example of versatile colliders and detectors

major upgrades over the last twenty years to improve particle identification and vertex reconstruction and is still evolving with an extension to forward rapidity as of today. pioneered in using new technologies: MRPC, MAPS, GEM and siPM.  
 Estimate 35M(initial) +75M(upgrades)\$.

RHIC energies, species combinations and luminosities (Run-1 to 22)



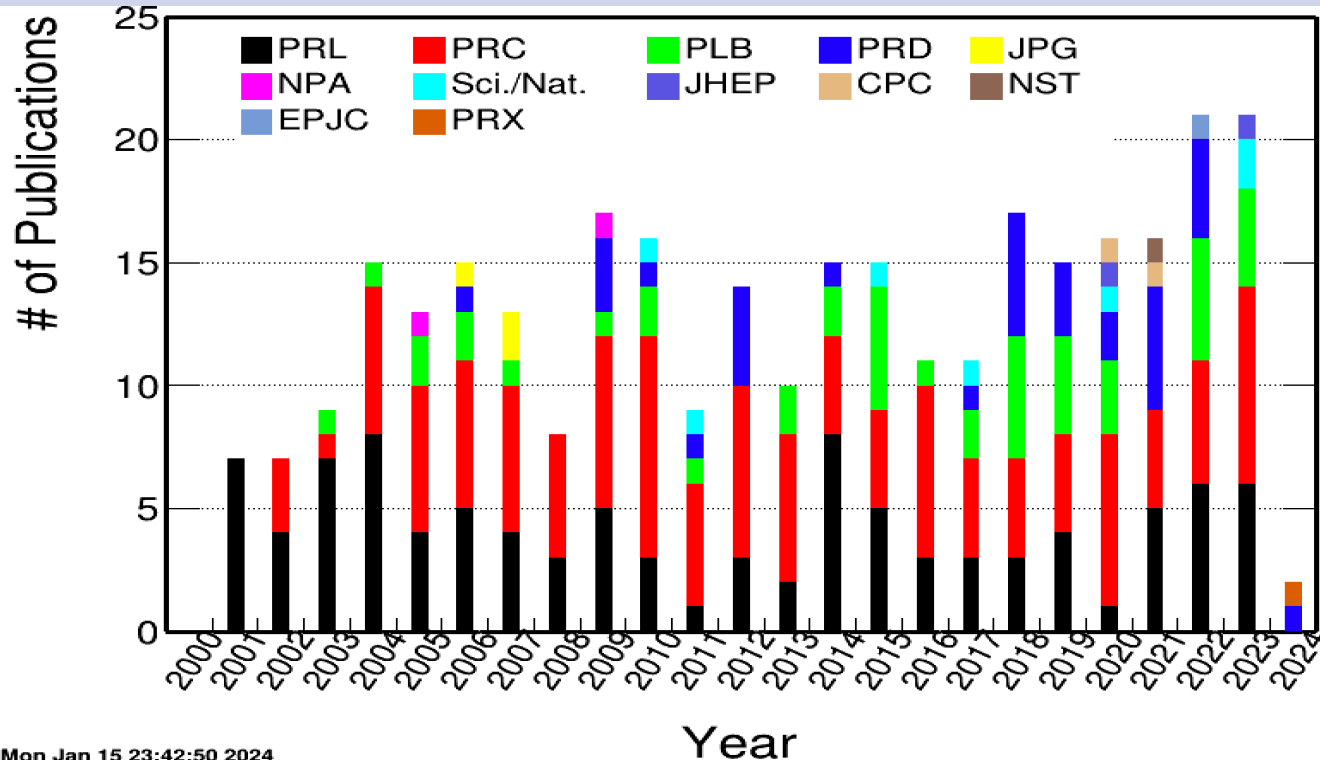
Detector	primary functions	DOE+(in-kind)	year
TPC+Trigger	$ \eta  < 1$ Tracking		1999-
Barrel EMC	$ \eta  < 1$ jets/ $\gamma/\pi^0/e$		2004-
FTPC	forward tracking	(Germany)	2002-2012
L3	Online Display	(Germany)	2000-2012
SVT/SSD	V0/charm	(France)	2004-2007
PMD	forward photons	(India)	2003-2011
EEMC	$1 < \eta < 2$ jets/ $\pi^0/e$	(NSF)	2005-
Roman Pots	diffractive		2009-
TOF	PID	(China)	2009-
FMS/Preshower	$2.5 < \eta < 4.2$	(Russia)	2008-2017
DAQ1000	x10 DAQ rate		2008-
HLT	Online Tracking	(China/Germany)	2012-
FGT	$1 < \eta < 2$ $W^\pm$		2012-2013
GMT	TPC calibration		2012-
HFT/SSD	open charm	(France/UIC)	2014-2016
MTD	muon ID	(China/India)	2014-
EPD	event plane	(China)	2018-
RHICf	$\eta > 5$ $\pi^0$	(Japan)	2017
iTPC	$ \eta  < 1.5$ Tracking	(China)	2019-
eTOF	$-2 < \eta < -1$ PID	(Germany/China)	2019-
FCS	$2.5 < \eta < 4$ calorimeter	(NSF)	2021-
FTS	$2.5 < \eta < 4$ Tracking	(NCKU/SDU)	2021-

8 new detectors added to STAR in last decade



# Eras defined in STAR

2000-2004	2005-2009	2010-2014	2014-2016	2017-2021	2022-2025
TPC	EMC	TOF+DAQ1K	HFT+MTD	iTPC+EPD+eTOF	fSTAR
QGP discovery	Jet, NPE, flow harmonics	BES-I (Critical Point); Symmetries: CME, EM probes	Open charm and Quarkonia	BES-II (Critical Point); Symmetries+DOF (isobar, Vorticity); Small Systems; FXT	Early-time dynamics; Imagining (2EIC); Statistics/precision nPDF
Transverse Spin Asymmetry Non-zero Gluon Spin Contribution to proton spin			Universality (sign change) Precise TMD over large phase space		



## Early-time dynamics:

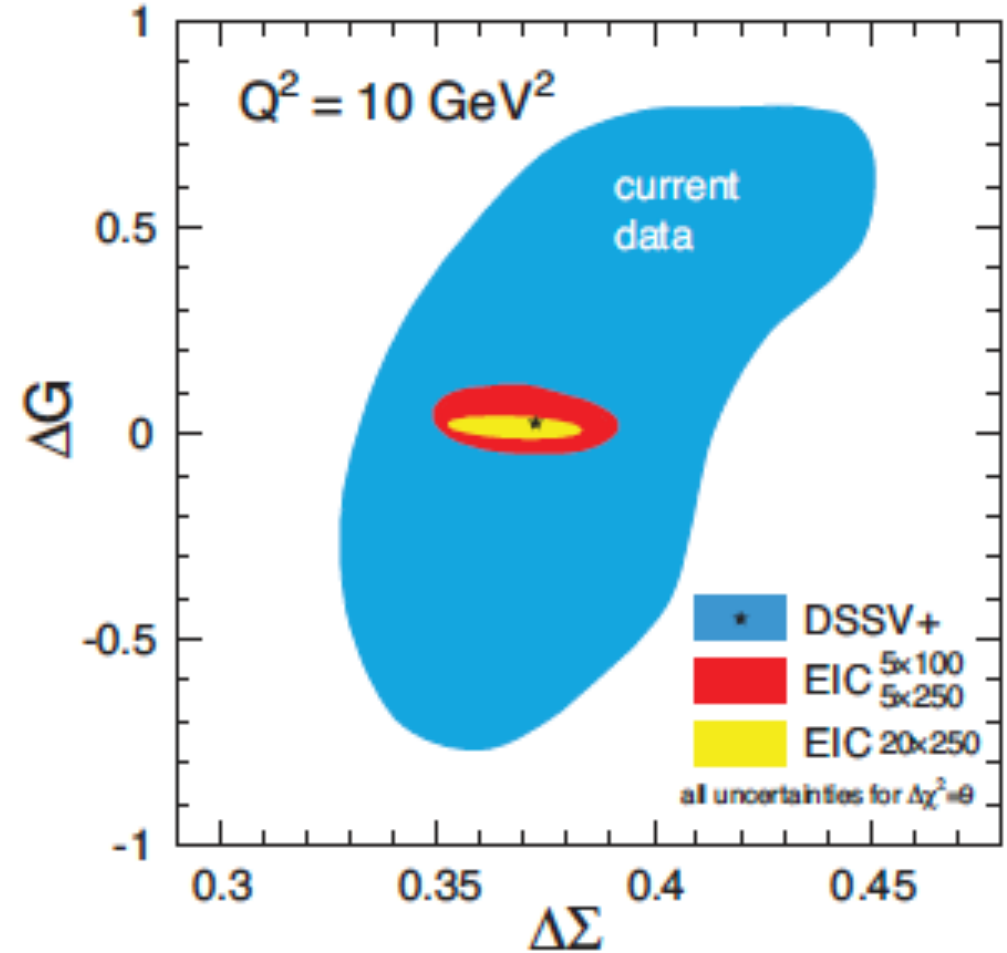
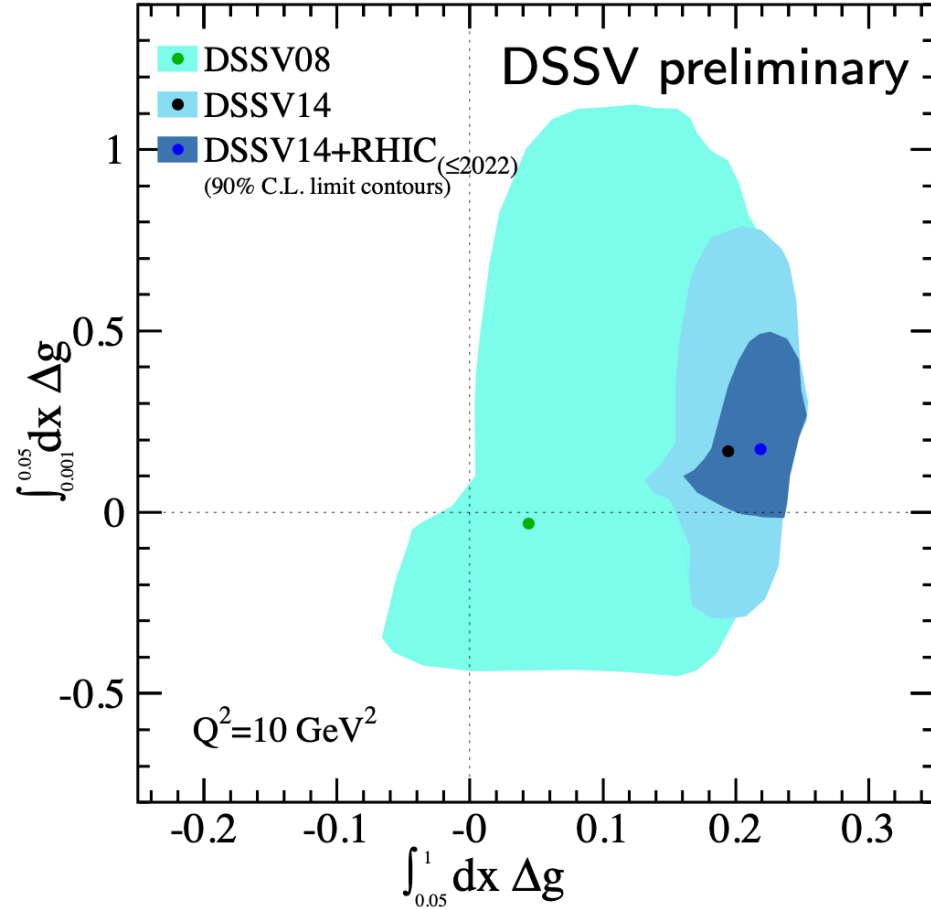
- Rapidity (de)correlations,
- Global Polarization in rapidity,
- Photon collisions;

## High statistics and precision:

- Higher order cumulants,
- Data points in Phase diagram,
- Jet structures and angles,
- Quarkonium flow

## Connections to EIC and FAIR

# One of the most direct connections to EIC physics



- RHIC data significantly improve  $\Delta G$  compared to 2008 results:

$$\int_{0.05}^1 dx \Delta g = 0.22 \pm 0.03, \text{ for } x > 0.05 \text{ and } Q^2 = 10 \text{ GeV}^2$$

- The white paper of the RHIC cold QCD program: E.C. Aschenauer et al., arXiv:2302.00605
- The EIC white paper: A. Accardi et al., arXiv:1212.1701



# Transverse Momentum Dependence (TMD) Parton Distribution Function (PDF) and Fragmentation Function (FF)

- quantitative comparisons of the validity and the limits of factorization and universality in lepton-proton and proton-proton collisions for initial and final state TMDs

Test of Siverson non-universality:  $Sivers_{SiDIS} = - Sivers_{DY, W^{+/-}, Z^0}$ ; Full jet and dijet Siverson asymmetry

Probe final state TMDs: Collins asymmetry for hadrons in jet

## Requirement:

- large data sets  $\sqrt{s} = 200$  and  $500$  GeV  $p \uparrow p$   
→ low to high  $x$ , highest and lowest  $x$  with fSTAR
- $A_{UT}$  for  $W^{+/-} Z^0$ ,  $A_{UT}$  for hadrons in jet

- First look Gluon GPD →  $E_g$

## Requirement:

- data sets  $\sqrt{s} = 500$  GeV  $p \uparrow p$  and  $\sqrt{s} = 200$  GeV  $p \uparrow A$
- $A_{UT}$  for  $J/\psi$  in UPC

- Physics driving the large  $A_N$  at forward rapidities and high  $x_F$

## Requirement:

- large data sets  $\sqrt{s} = 200$  and  $500$  GeV  $p \uparrow p$   
→ low to highest  $x_F$  → fSTAR
- charge hadron  $A_N$  at forward rapidities

- Nuclear dependence of PDFs, FF, and TMDs

## Requirement:

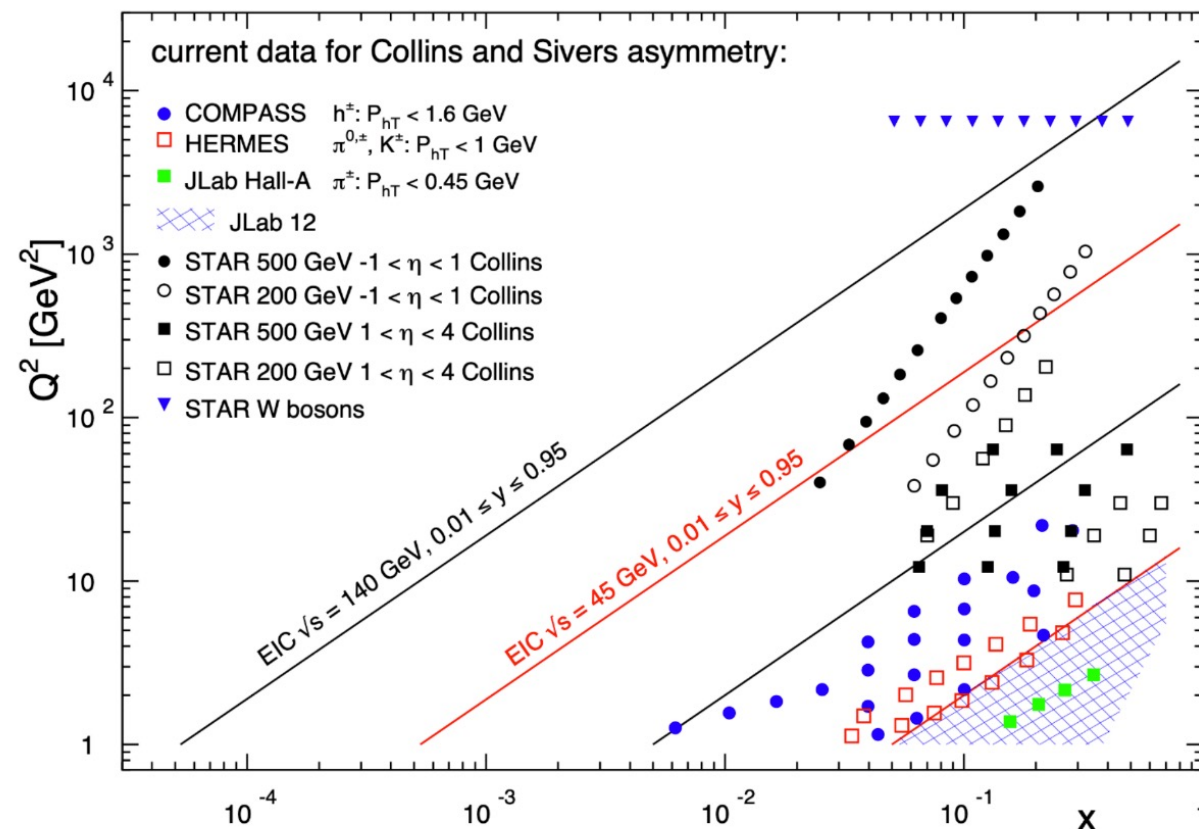
- large equal data set of  $\sqrt{s} = 200$   $p \uparrow p$  and  $p \uparrow Au$   
→ low to high  $x$ , highest and lowest  $x$  with fSTAR
- $R_{pA}$  direct photons and DY, hadrons in jet  $A_{UT}$

- non-linear effects in QCD

## Requirement:

- large equal data set of  $\sqrt{s} = 200$   $p \uparrow p$  and  $p \uparrow Au$   
→ lowest- $x$  through fSTAR
- dihadron correlations for  $h^{+/-}$ ,  $\gamma$ -jet, di-jets

- STAR@RHIC Unique Kinematics
- Cover large  $Q^2$  and  $x$  range
- Significant overlap with EIC kinematics
- Different tools and beam energies:  
 $W^\pm/Z$ , DY g, jet,  $p^\pm/p^0$ , two-hadron correlations



# Transverse Momentum Dependence (TMD) Parton Distribution Function and Fragmentation Function

- quantitative comparisons of the validity and the limits of factorization and universality in lepton-proton and proton-proton collisions for initial and final state TMDs

Test of Sivers non-universality:  $Sivers_{SiDIS} = - Sivers_{DY, W^{\pm}, Z^0}$ ; Full jet and dijet Sivers asymmetry

Probe final state TMDs: Collins asymmetry for hadrons in jet

- Requirement:

- large data sets  $\sqrt{s} = 200$  and  $500$  GeV  $p \uparrow p$ 
  - low to high  $x$ , highest and lowest  $x$  with fSTAR
- $A_{UT}$  for  $W^{\pm}, Z^0$ ,  $A_{UT}$  for hadrons in jet

- First look Gluon GPD →  $E_g$

- Requirement:

- data sets  $\sqrt{s} = 500$  GeV  $p \uparrow p$  and  $\sqrt{s} = 200$  GeV  $p \uparrow A$
- $A_{UT}$  for  $J/\psi$  in UPC

- Physics driving the large  $A_N$  at forward rapidities and high  $x_F$

- Requirement:

- large data sets  $\sqrt{s} = 200$  and  $500$  GeV  $p \uparrow p$ 
  - low to highest  $x_F$  → fSTAR
- charge hadron  $A_N$  at forward rapidities

- Nuclear dependence of PDFs, FF, and TMDs

- Requirement:

- large equal data set of  $\sqrt{s} = 200$   $p \uparrow p$  and  $p \uparrow Au$ 
  - low to high  $x$ , highest and lowest  $x$  with fSTAR
- $R_{pA}$  direct photons and DY, hadrons in jet  $A_{UT}$

- non-linear effects in QCD

- Requirement:

- large equal data set of  $\sqrt{s} = 200$   $p \uparrow p$  and  $p \uparrow Au$ 
  - lowest- $x$  through fSTAR
- dihadron correlations for  $h^{\pm}, \gamma$ -jet, di-jets

- STAR@RHIC Unique Kinematics
- Cover large  $Q^2$  and  $x$  range
- Significant overlap with EIC kinematics
- Different tools and beam energies:  
 $W^{\pm}/Z$ , DY g, jet,  $p^{\pm}/p^0$ , two-hadron correlations

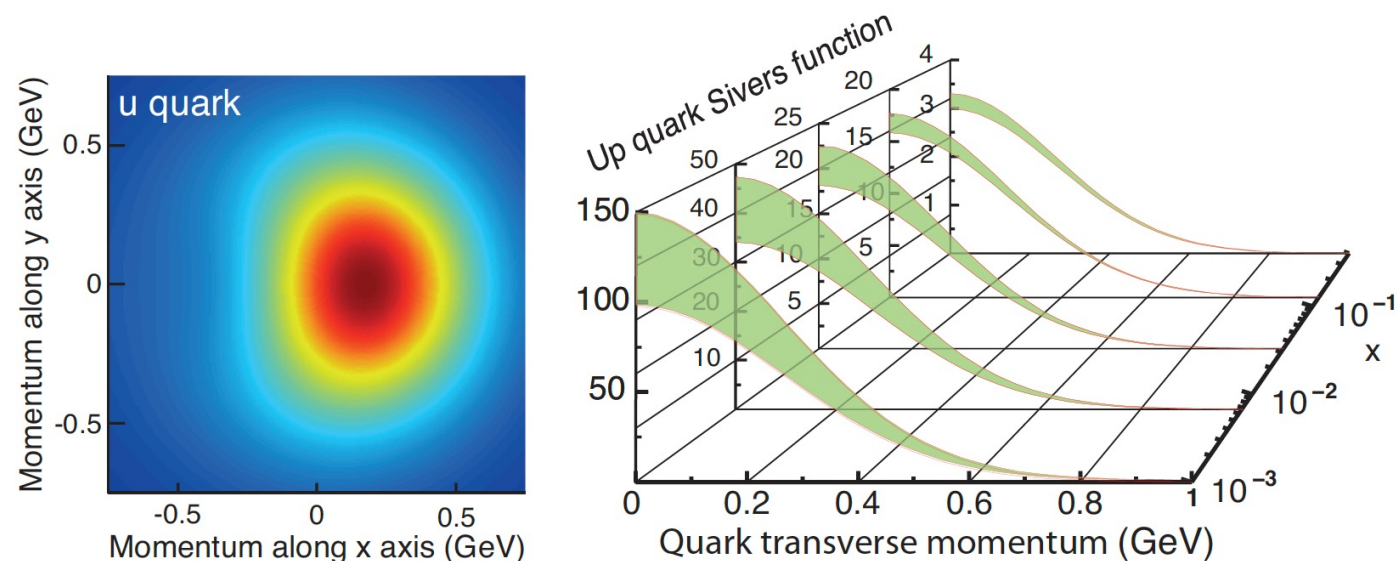


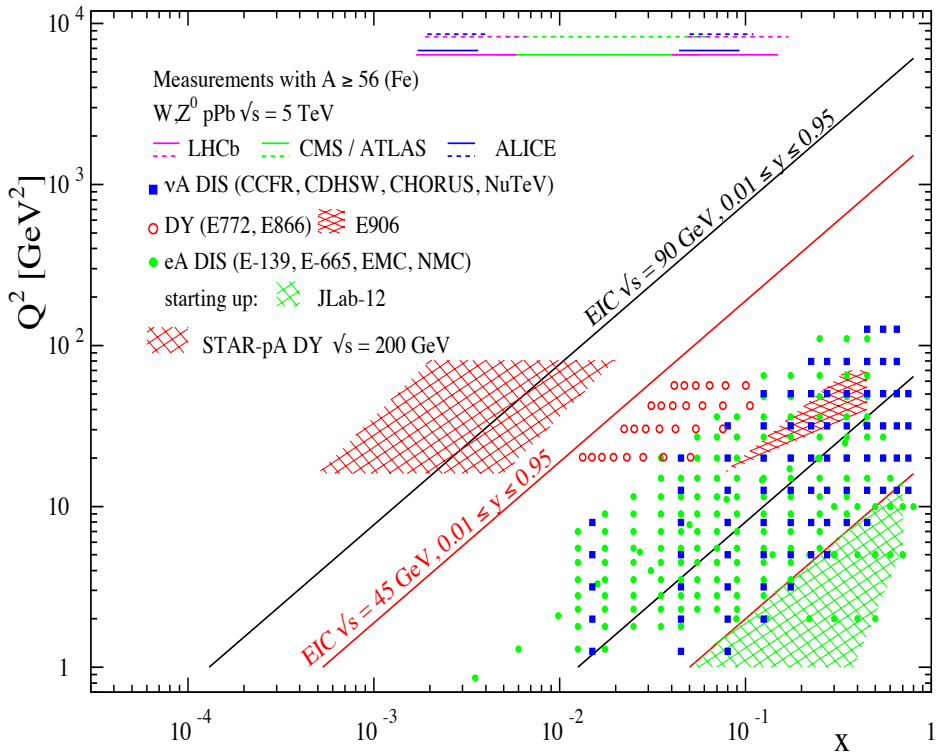
Figure 1.3: **Left:** The transverse-momentum distribution of an up quark with longitudinal momentum fraction  $x = 0.1$  in a transversely polarized proton moving in the  $z$ -direction, while polarized in the  $y$ -direction. The color code indicates the probability of finding the up quarks. **Right:** The transverse-momentum profile of the up quark Sivers function at five  $x$  values accessible to the EIC, and corresponding statistical uncertainties.

# Nuclear PDF and Initial Conditions for A+A collisions

measure nPDF in a  $x$ - $Q^2$  region where nuclear effects are large

$$Q^2 > Q_s^2 \text{ over a wide range in } x$$

**pA@RHIC: unique kinematics**



STAR Forward upgrade with tracking and calorimeters  
Cold QCD/ Spin physics

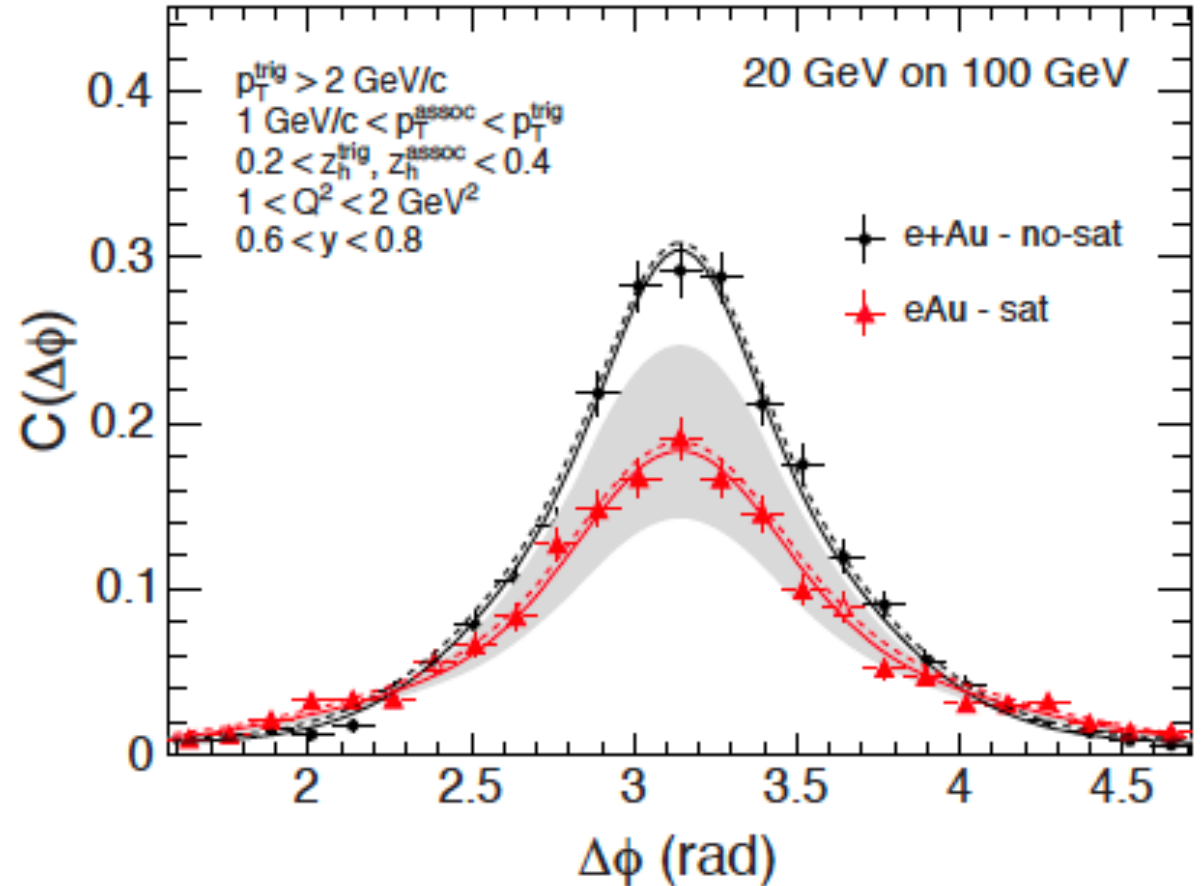
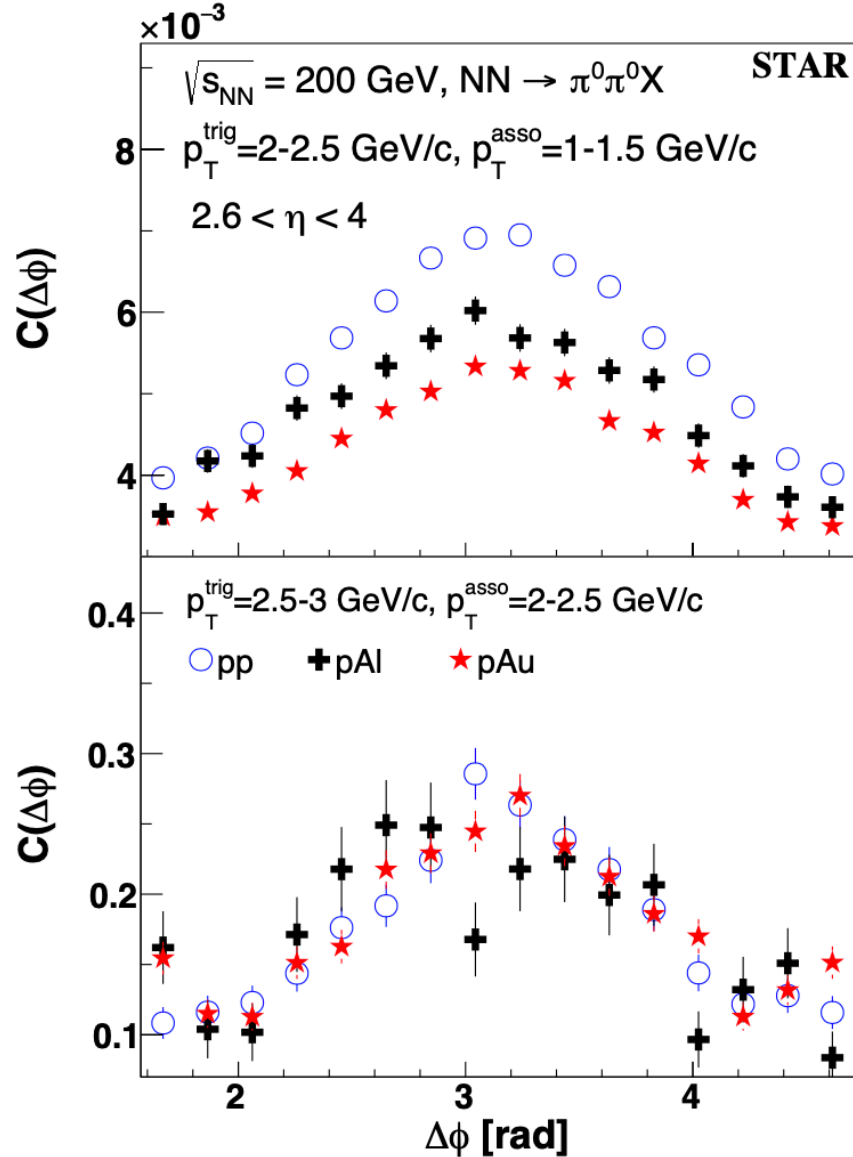
	Year	$\sqrt{s}$ (GeV)	Delivered Luminosity	Scientific Goals	Observable	Required Upgrade
Scheduled RHIC running	2023 to 2025	p <sup>+</sup> p @ 200	300 pb <sup>-1</sup> 8 weeks	Subprocess driving the large $A_N$ at high $x_F$ and $\eta$	$A_N$ for charged hadrons and flavor enhanced jets	Forward instrum. ECal+HCal+Tracking
		p <sup>+</sup> Au @ 200	1.8 pb <sup>-1</sup> 8 weeks	What is the nature of the initial state and hadronization in nuclear collisions	$R_{pAu}$ direct photons and DY	Forward instrum. ECal+Hcal+Tracking
		p <sup>+</sup> Al @ 200	12.6 pb <sup>-1</sup> 8 weeks	Clear signatures for Saturation A-dependence of nPDF, A-dependence for Saturation	Dihadrons, $\gamma$ -jet, h-jet, diffraction $R_{pAl}$ direct photons and DY Dihadrons, $\gamma$ -jet, h-jet, diffraction	Forward instrum. ECal+HCal+Tracking
	AuAu @ 200	1 Billion Minbias Events	Longitudinal de-correlation	$C_n(\Delta\eta)$ and $r_n(\eta_s, \eta_b)$	Forward instrum. ECal+HCal or Tracking	
		$\eta/s(T)$ and $\zeta/s(T)$	$V_{n\Delta}(\eta)$	Forward instrum. Tracking		
		Mixed flow Harmonics	$C_{m,n,m+n}$	Forward instrum. ECal+HCal or Tracking		
Rapidity dependence of Hyperon Polarization	$P_H(\eta)$	Forward instrum. Tracking				
Ridge	$dN/d(\Delta\eta)d(\Delta\phi) \& V_{n\Delta}$	Forward instrum. ECal+HCal or Tracking				
Potential future running	2021	p <sup>+</sup> p @ 510	1.1 fb <sup>-1</sup> 10 weeks	TMDs at low and high $x$	$A_{UT}$ for Collins observables, i.e. hadron in jet modulations at $\eta > 1$	Forward instrum. ECal+HCal+Tracking
2021	$\bar{p}$ <sup>+</sup> $\bar{p}$ @ 510	1.1 fb <sup>-1</sup> 10 weeks	$\Delta g(x)$ at small $x$	$A_{UU}$ for jets, di-jets, h/ $\gamma$ -jets at $\eta > 1$	Forward instrum. ECal+HCal	



# Gluon Non-linear/Saturation Effect

STAR, Phys. Rev. Lett. **129** (2022) 92501;  
arXiv: 2111.10396

Projection: EIC Whitepaper Fig.3.18



$2\pi$  correlations at STAR forward shows  
suppression of yield with increase nuclear mass A  
shape does not change

# A picture is worth a thousand words

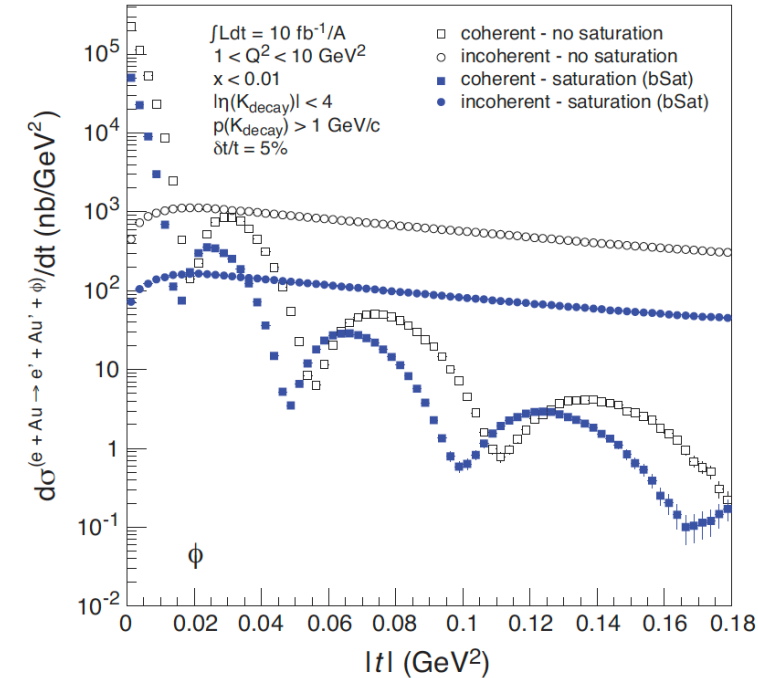
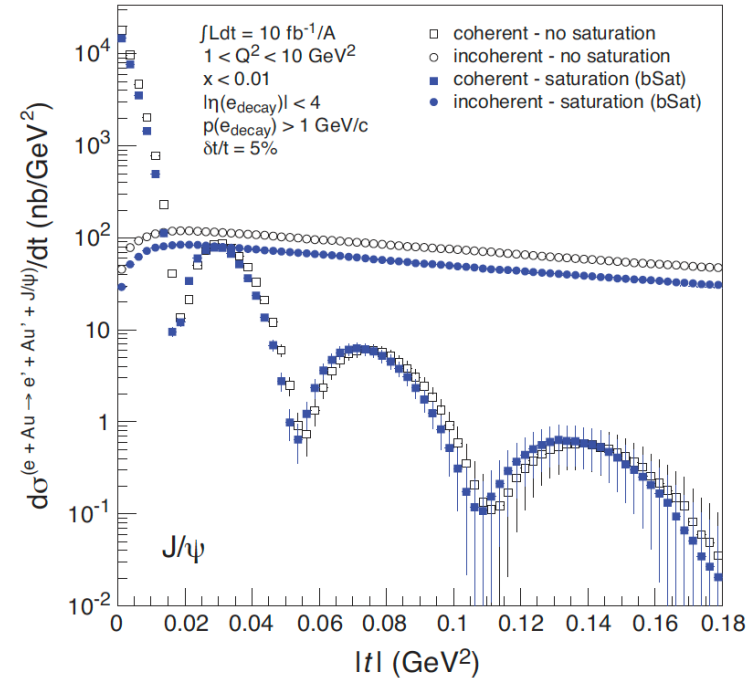
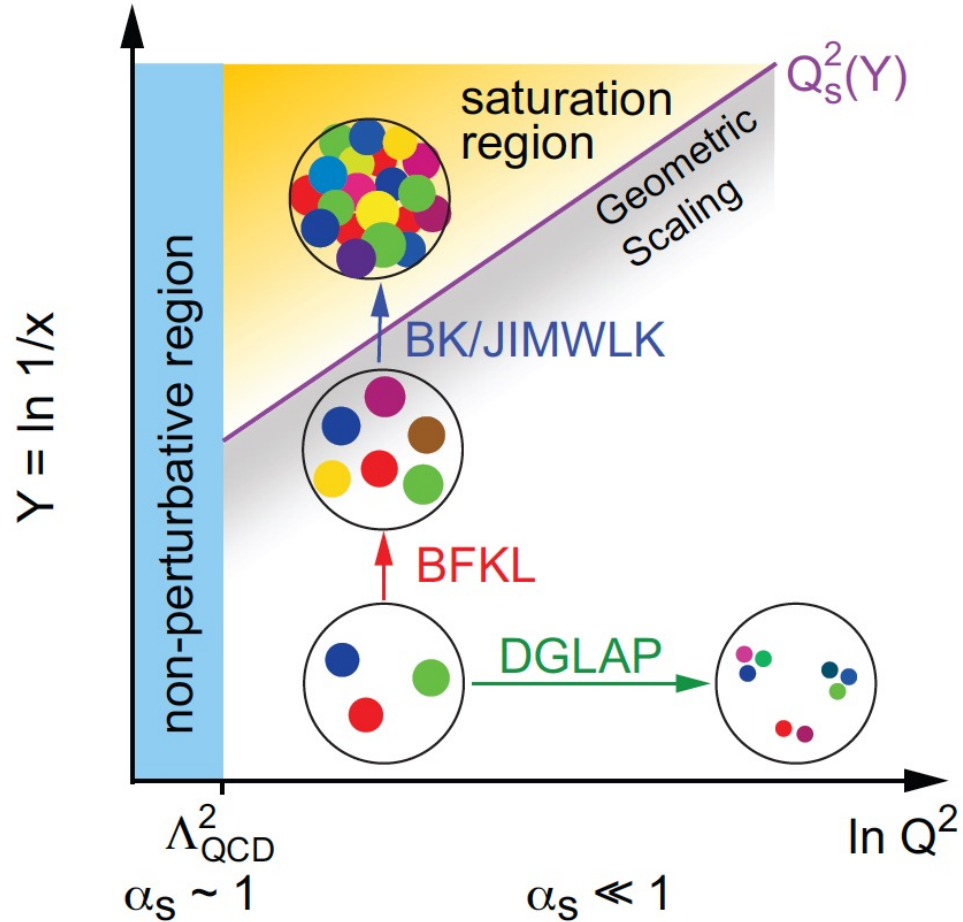


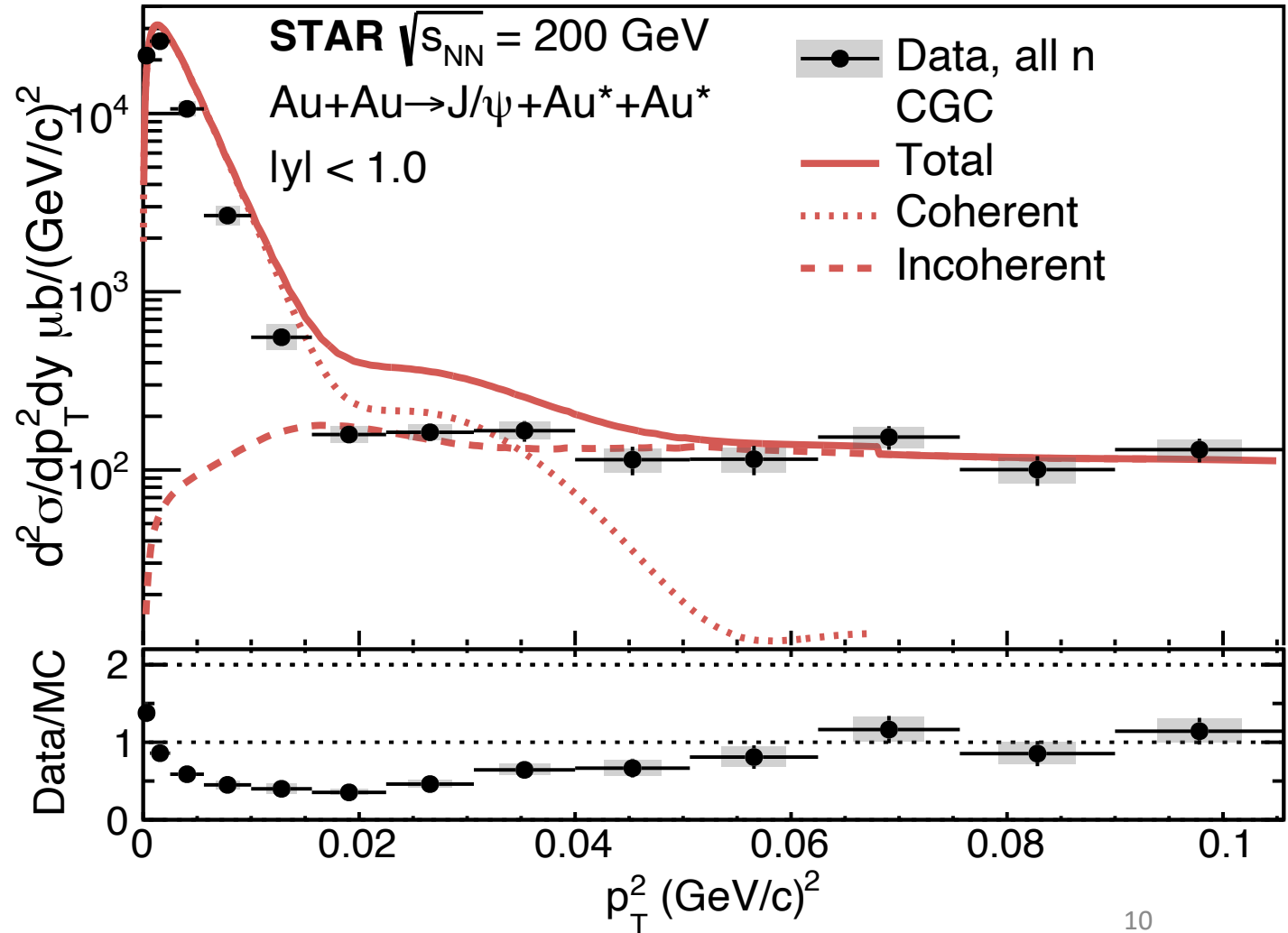
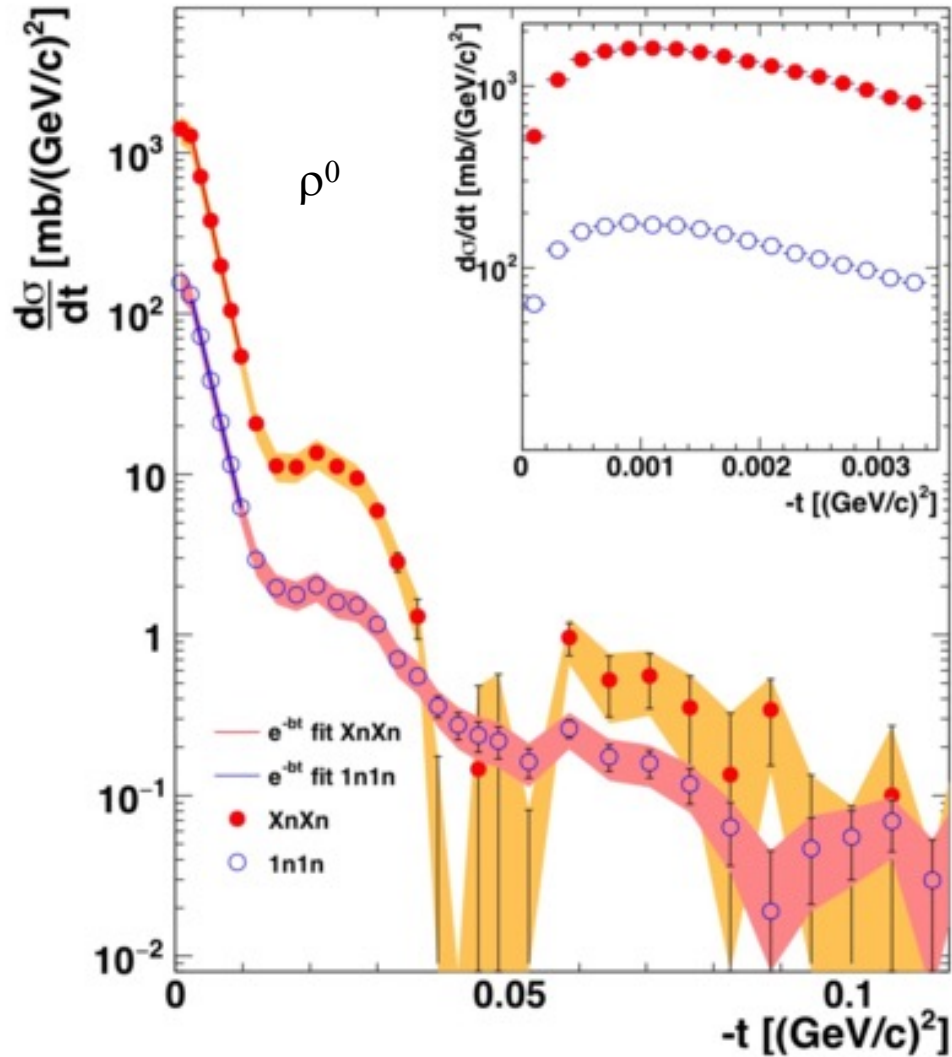
Figure 3.23:  $d\sigma/dt$  distributions for exclusive  $J/\psi$  (left) and  $\phi$  (right) production in coherent and incoherent events in diffractive  $e+Au$  collisions. Predictions from saturation and non-saturation models are shown.

Imaging of 3D gluon distribution of heavy ion at high density (low-x)

# Vector Meson diffractive production in UPC

STAR, Phys. Rev. C **96** (2017) 54904

STAR, arXiv:2311.13632, 2311.13637





# Spin Interference Enabled Nuclear Tomography

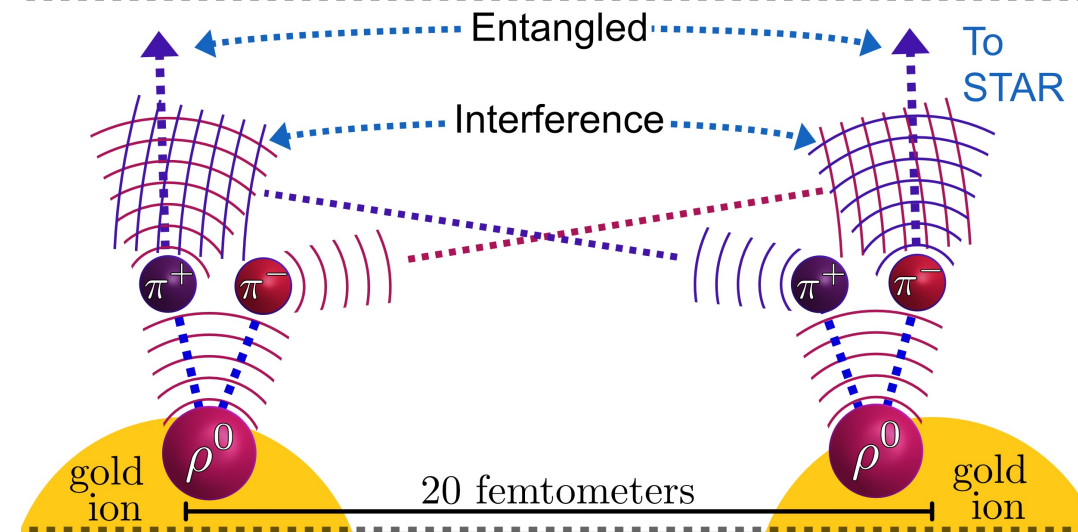
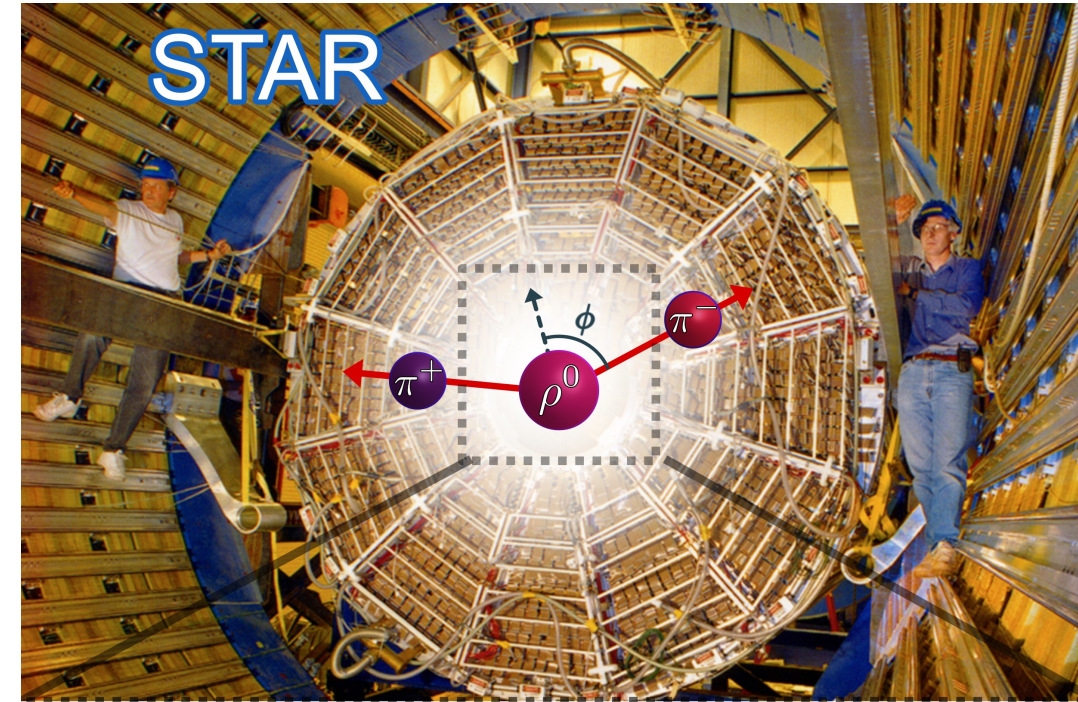
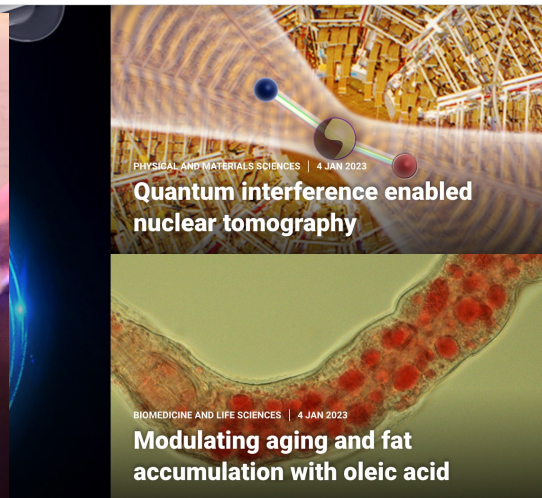
STAR, arXiv:2204.01625

- Teaser:  
Polarized photon-gluon fusion reveals quantum wave interference of non-identical particles and shape of high-energy nuclei

ScienceAdvances

Current Issue First release papers Archive About Submit manuscript

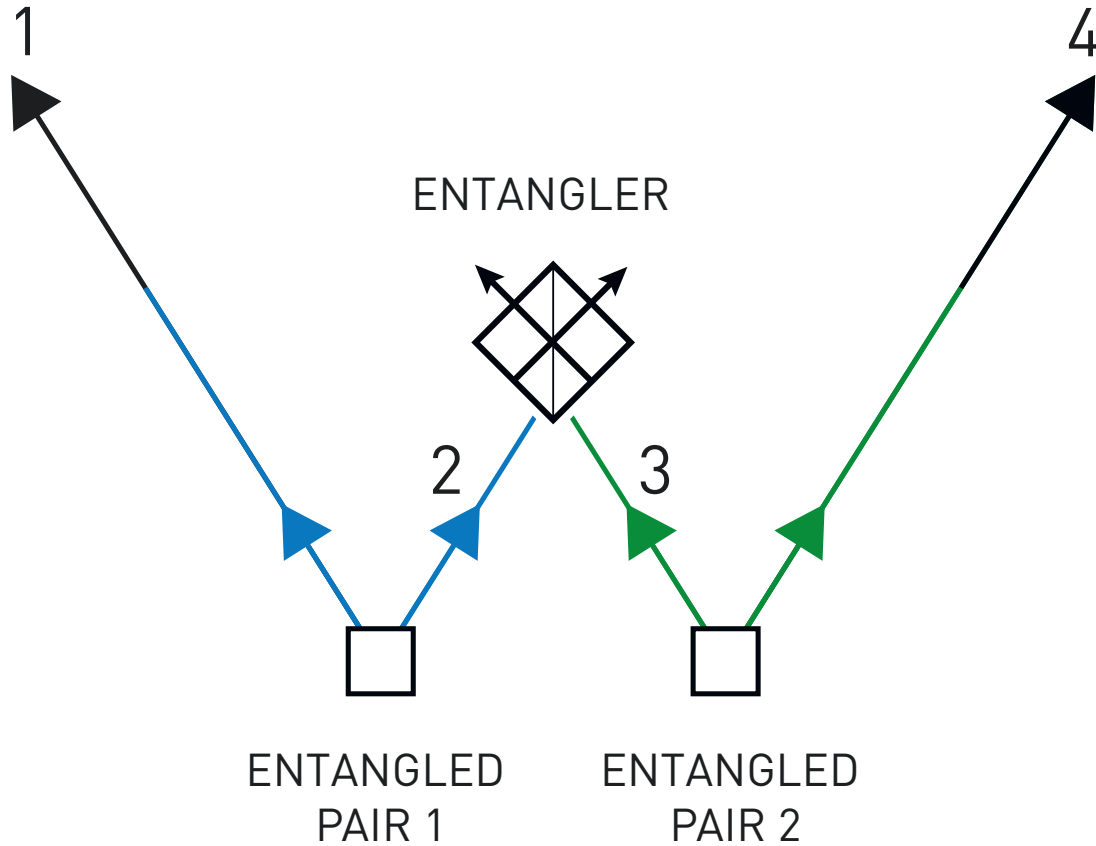
GET OUR E-ALERTS



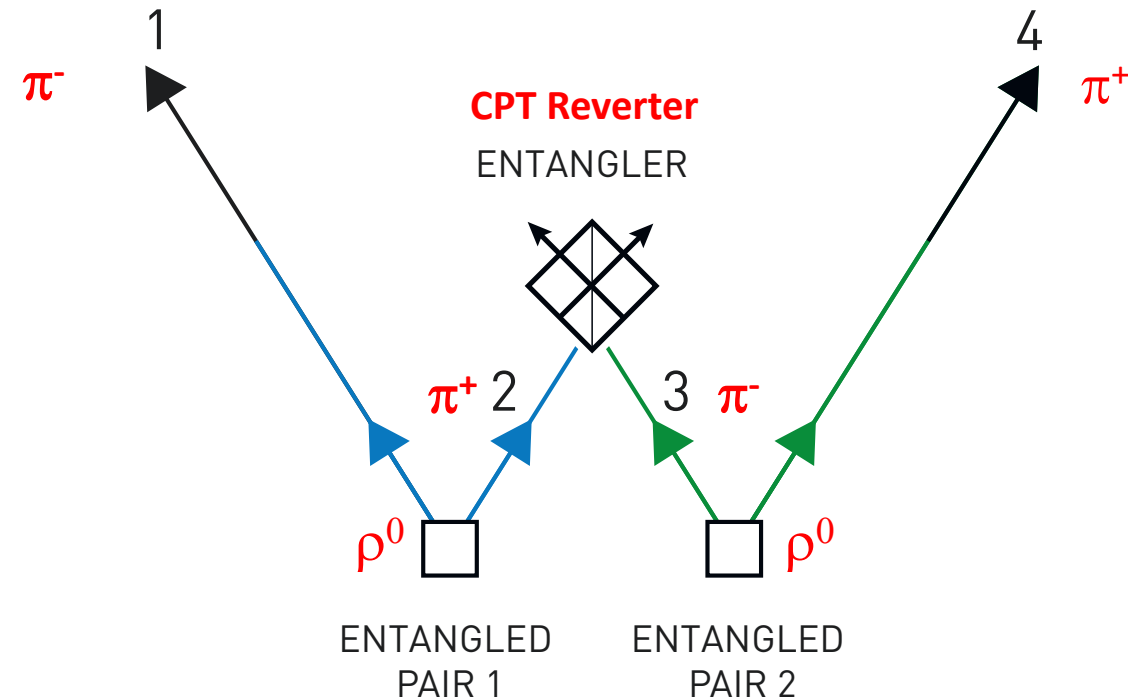
# Entangled particles that never met

Two pairs of entangled particles are emitted from different sources. One particle from each pair is brought together in a special way that entangles them. The two other particles (1 and 4 in the diagram) are then also entangled. In this way, two particles that have never been in contact can become entangled.

Nobel Prize in Physics 2022



Since  $\pi^+$  and  $\pi^-$  are particle and antiparticle of each other, their wavefunctions could "annihilate"?





# Entangled particles that never met

Two pairs of entangled particles are emitted from different sources. One particle from each pair meets the other particle from the other pair. In this way, two

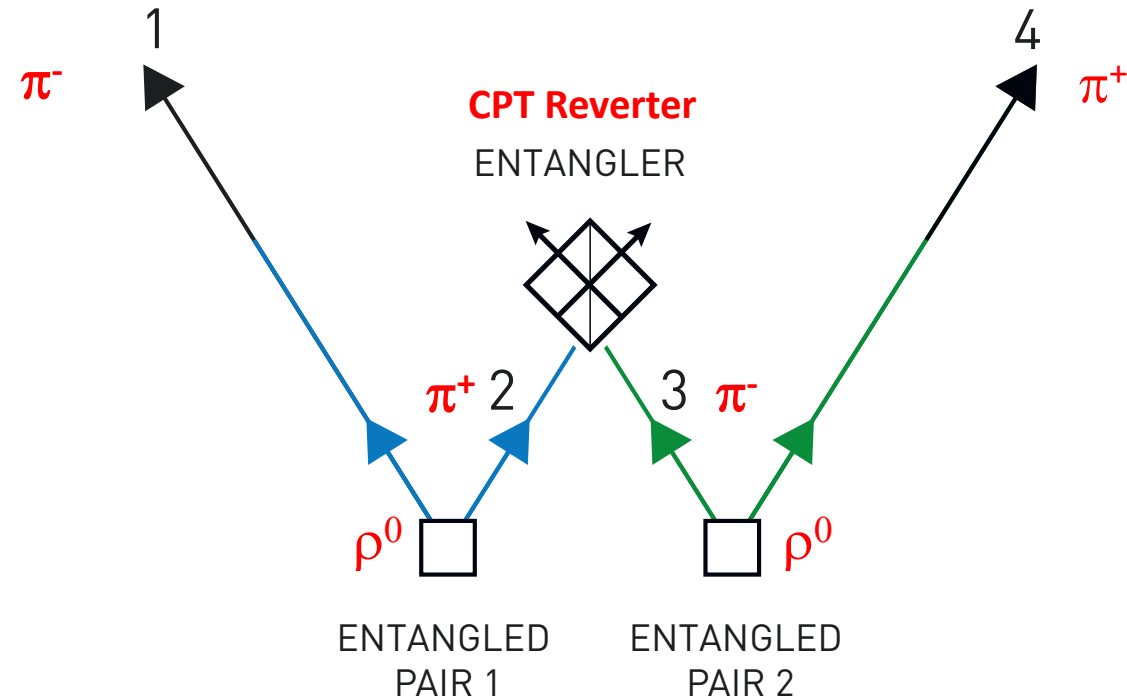
$$|\pi^-\rangle = |\pi_1^-\rangle e^{i\phi_1} + |\pi_2^-\rangle e^{i\phi_2}$$

$$|\pi^+\rangle = |\pi_1^+\rangle e^{i\phi_1} + |\pi_2^+\rangle e^{i\phi_2}$$

$$\begin{aligned} |\pi^-\rangle |\pi^+\rangle &= (|\pi_1^-\rangle e^{i\phi_1} + |\pi_2^-\rangle e^{i\phi_2}) (|\pi_1^+\rangle e^{i\phi_1} + |\pi_2^+\rangle e^{i\phi_2}) \\ &= (|\pi_1^-\rangle |\pi_1^+\rangle e^{i2\phi_1} + |\pi_2^-\rangle |\pi_2^+\rangle e^{i2\phi_2} \\ &\quad + |\pi_1^-\rangle |\pi_2^+\rangle e^{i(\phi_1+\phi_2)} + |\pi_2^-\rangle |\pi_1^+\rangle e^{i(\phi_1+\phi_2)}) \end{aligned}$$

$$\begin{aligned} \langle \pi^- | \pi^+ \rangle &= (\langle \pi_1^- | \langle \pi_2^- | e^{-i2\phi_1} + \langle \pi_1^- | \langle \pi_2^- | e^{-i2\phi_2} \\ &\quad + \langle \pi_1^- | \langle \pi_2^+ | e^{-i(\phi_1+\phi_2)} + \langle \pi_2^- | \langle \pi_1^+ | e^{-i(\phi_1+\phi_2)})} \\ &\quad (|\pi_1^-\rangle |\pi_1^+\rangle e^{i2\phi_1} + |\pi_2^-\rangle |\pi_2^+\rangle e^{i2\phi_2} \\ &\quad + |\pi_1^-\rangle |\pi_2^+\rangle e^{i(\phi_1+\phi_2)} + |\pi_2^-\rangle |\pi_1^+\rangle e^{i(\phi_1+\phi_2)}) \\ &= \langle \pi_1^- | \pi_1^- \rangle \langle \pi_1^+ | \pi_1^+ \rangle + \langle \pi_2^- | \pi_2^- \rangle \langle \pi_2^+ | \pi_2^+ \rangle \\ &\quad + \langle \pi_1^- | \pi_1^- \rangle \langle \pi_2^+ | \pi_2^+ \rangle + \langle \pi_2^- | \pi_2^- \rangle \langle \pi_1^+ | \pi_1^+ \rangle \\ &\quad + \langle \pi_2^- | \pi_1^- \rangle \langle \pi_1^+ | \pi_2^+ \rangle + \langle \pi_2^- | \pi_2^- \rangle \langle \pi_1^+ | \pi_1^+ \rangle \end{aligned}$$

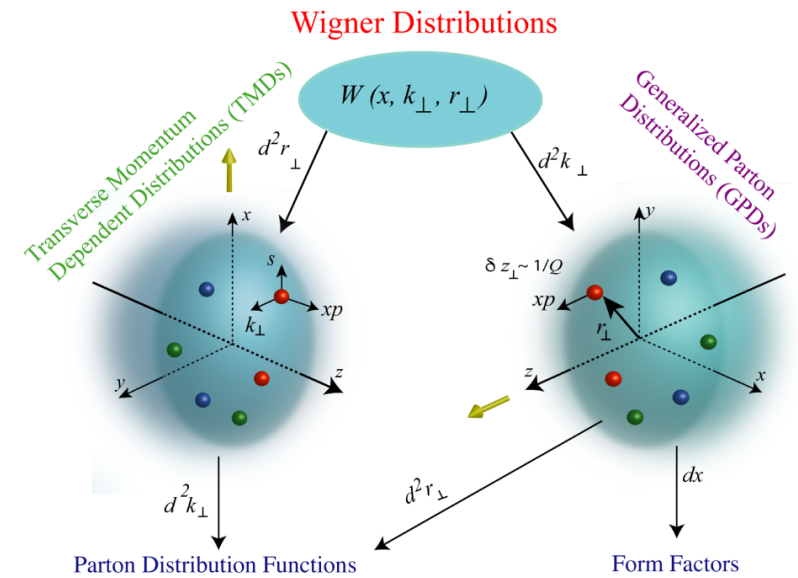
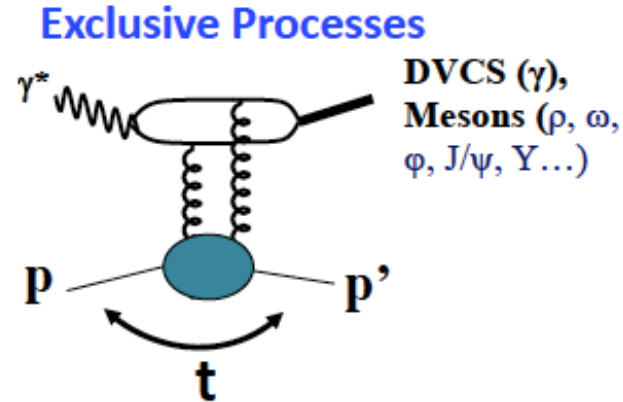
Since  $\pi^+$  and  $\pi^-$  are particle and antiparticle of each other, their wavefunctions could "annihilate"?





# New observable in $\rho$ photoproduction

- Predicted to be sensitive to Generalized Transverse Momentum Distribution (GTMD):  
“offer direct access to the second derivative of the saturation scale w.r.t gluon spatial distribution”

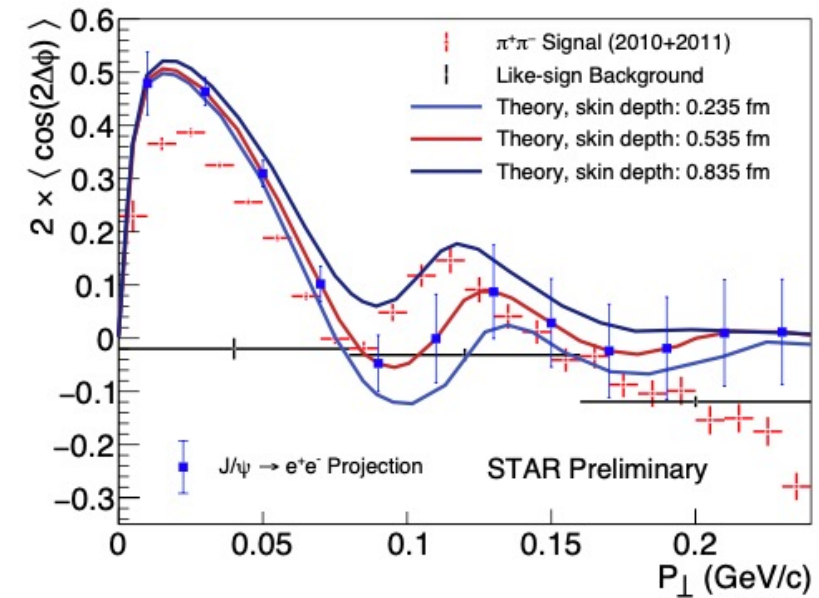
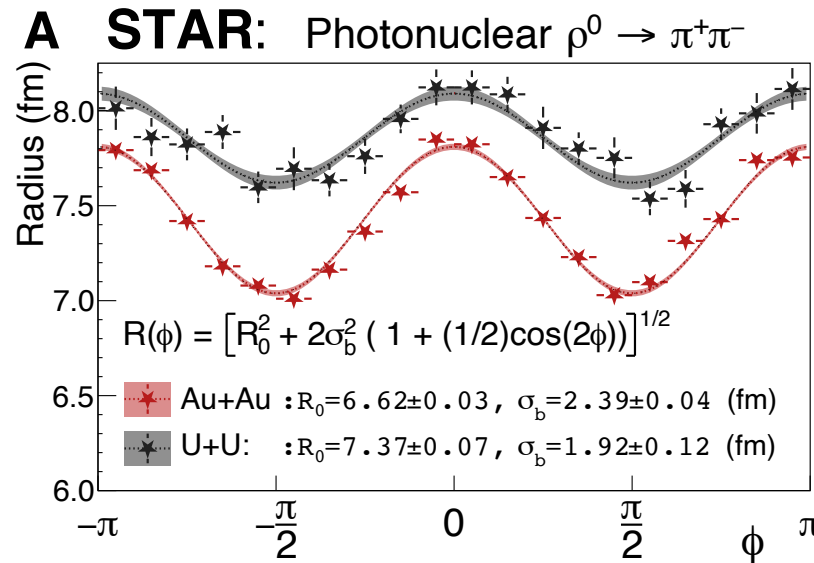


- Expected magnitude scales with  $(P_\perp/M_\rho)^2$
- Tensor Pomeron ...

[1] J. Zhou, Phys. Rev. D 94 (2016) 114017;

A. Metz *et al.*, PRD 84 (2011) 051503

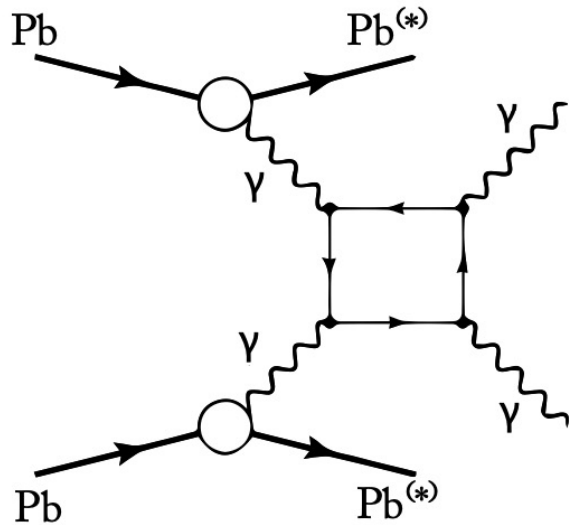
[“Distribution of linearly polarized gluons inside a large nucleus”](#)



**Observations of  $\cos(2\phi)$  modulation  $\rightarrow$  photons are polarized**  
**Observations of  $\cos(4\phi)$  modulation  $\rightarrow$  Linear polarized gluons have spatial gradient**

# Recent Discoveries in Ultra-peripheral collisions:

## 2017: Light-by-Light



[Open Access](#) | [Published: 14 August 2017](#)

**Evidence for light-by-light scattering in heavy-ion collisions with the ATLAS detector at the LHC**

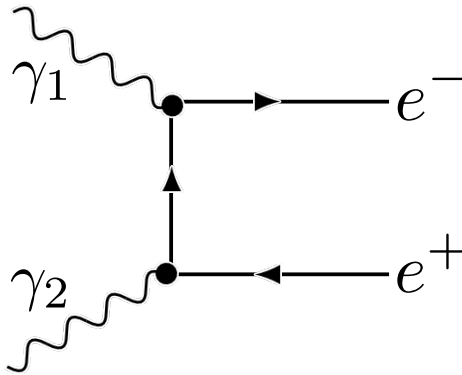
[ATLAS Collaboration](#)

[Nature Physics](#) **13**, 852–858 (2017) | [Cite this article](#)

41k Accesses | 185 Citations | 521 Altmetric | [Metrics](#)



## 2021: Breit-Wheeler



OUTPUTS FROM PHYSICAL REVIEW LETTERS

#42

of 37,322 outputs



## 2023: Entanglement Enabled Interference

**Science Advances**

AAAS

Article Metrics

[? What is this page?](#) [Embed badge](#) [Share](#)

Tomography of ultrarelativistic nuclei with polarized photon-gluon collisions

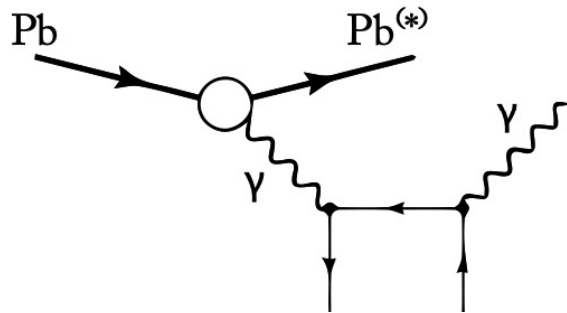
Overview of attention for article published in Science Advances, January 2023

## Scientists See Quantum Interference between Different Kinds of Particles for First Time

A newly discovered interaction related to quantum entanglement between dissimilar particles opens a new window into the nuclei of atoms

# Recent Discoveries in Ultra-peripheral collisions:

## 2017: Light-by-Light

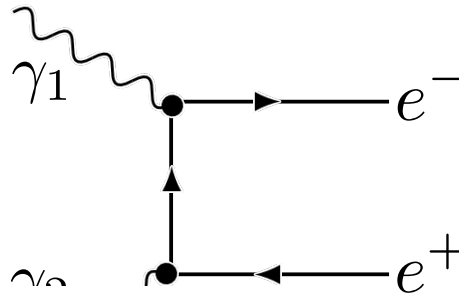


Understanding photon collisions could aid search for physics beyond the Standard Model

Phys.org, 20 Sep 2021

Hot on the heels of proving an 87-year-old prediction that matter can be generated directly from light, Rice University...

## 2021: Breit-Wheeler



## 2023: Entanglement Enabled Interference

Science Advances

AAAS

Article Metrics

What is this page? Embed badge Share

Tomography of ultrarelativistic nuclei with polarized photon-gluon collisions

Overview of attention for article published in Science Advances, January 2023

## Scientists See Quantum Interference between Different Kinds of Particles for First Time

A newly discovered interaction related to quantum entanglement between dissimilar particles opens a new window into the nuclei of atoms

PHYSICAL REVIEW LETTERS

42

322 outputs



成大高能核物理實驗室 參與愛因斯坦著名公式驗證

PC Home, 08 Sep 2021

【大成報/記者于郁金/臺南報導】國立成功大學高能核物理實驗室參與位在美國布魯克海文國家實驗室(Brookhaven National Laboratory, BNL)STAR實驗, 首次驗證從純能量(光子)產生正反物質對, 這就是愛因斯坦最著名的質能互換公式: E...

成大高能核物理實驗室 參與愛因斯坦著名公式驗

HiNet, 08 Sep 2021

【勤報/記者于郁金/臺南報導】國立成功大學高能核物理實驗室參與位在美國布魯克海文國家實驗室(Brookhaven National Laboratory, BNL)STAR實驗, 首次驗證從純能量(光子)產生正反物質對, 這就是愛因斯坦最著名的質能互換公式: E=m...

Revolutionäre Physik bestätigt 80 Jahre alte Theorie: Forscher wandeln Licht in Materie um

Trends DeZukunft, 23 Aug 2021

E=mc<sup>2</sup> – die berühmte Formel von Albert Einstein kennt so gut wie jeder. Die Erkenntnis dahinter ist wiederum wahrscheinlich...

Forscher erzeugen Materie aus Licht - Experiment im Teilchenbeschleuniger bestätigt fast 90 Jahre alte Theorie - scinexx.de

Scinexx, 22 Aug 2021

Einstein im Beschleuniger: Physiker haben Materieteilchen aus purem Licht erzeugt – durch die Kollision von energiereichen...

ate University



# Imaging the initial stages of heavy ion collisions

Extensive measurements from RHIC on different harmonics of azimuthal correlations have strongly constrained the modeling of initial stages of heavy ion collisions.

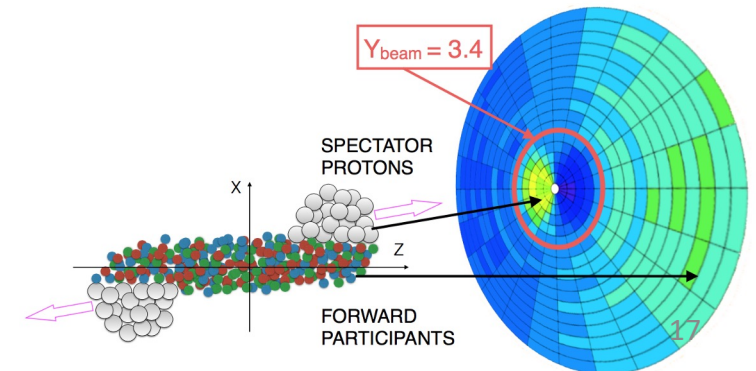
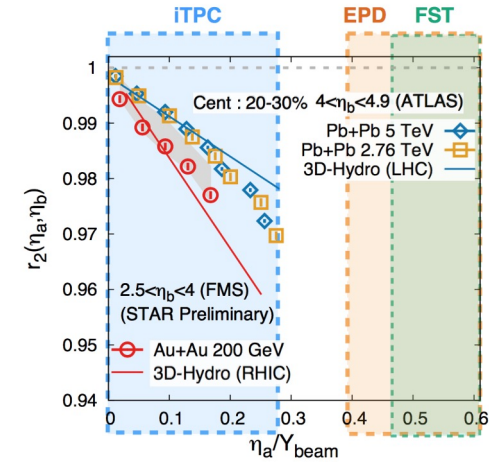
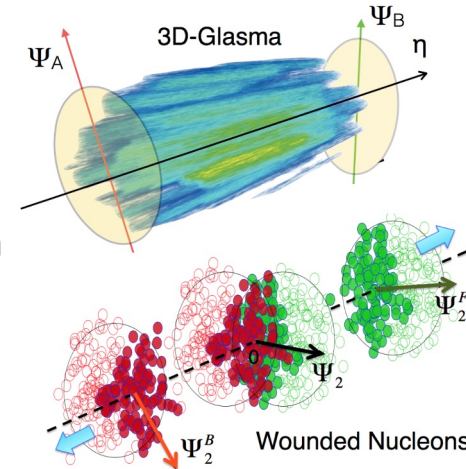
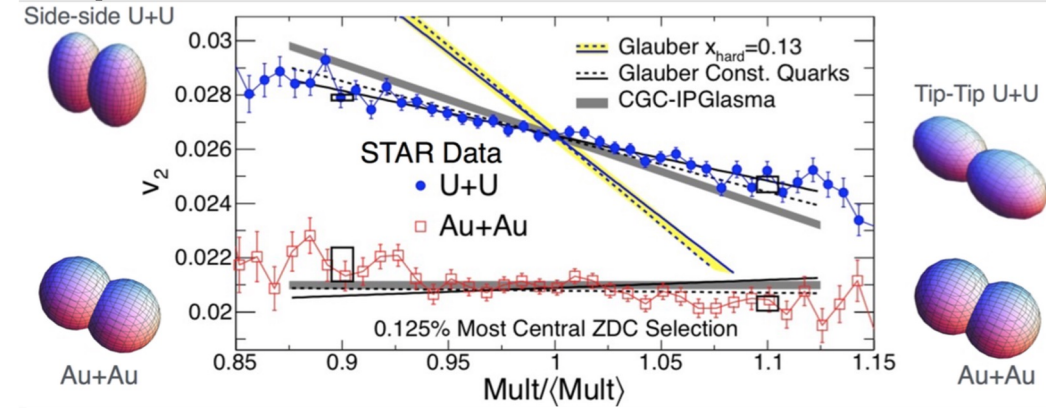
STAR Collaboration (L. Adamczyk et al.), *Phys. Rev. Lett.* **115**, 222301 (2015), *Phys. Rev. C* **98**, 034918 (2018), *Phys. Lett. B* **790** (2019) 81-88

**Past half decade (Au+Au, U+U, Cu+Au):** The shape of nuclei, geometry of collisions, various sources of initial state fluctuations, dynamics of initial state. **Constraints on state-of-the art modeling** of colliding nuclei before the era of EIC.

**Ongoing (Light-heavy ion, pAu, dAu, 3He+Au):** Role of subnucleon fluctuations in small collision systems:

**Ongoing (Measurements with Beam Energy Scan-II upgrades):**

Initial stages of colliding nuclei at lower energies (7.7-27 GeV), the role of valence dof or nucleon wavefunction inside a nucleus



# Imaging of nuclear shape at RHIC

STAR, arXiv:2401.06625, submitted to Nature

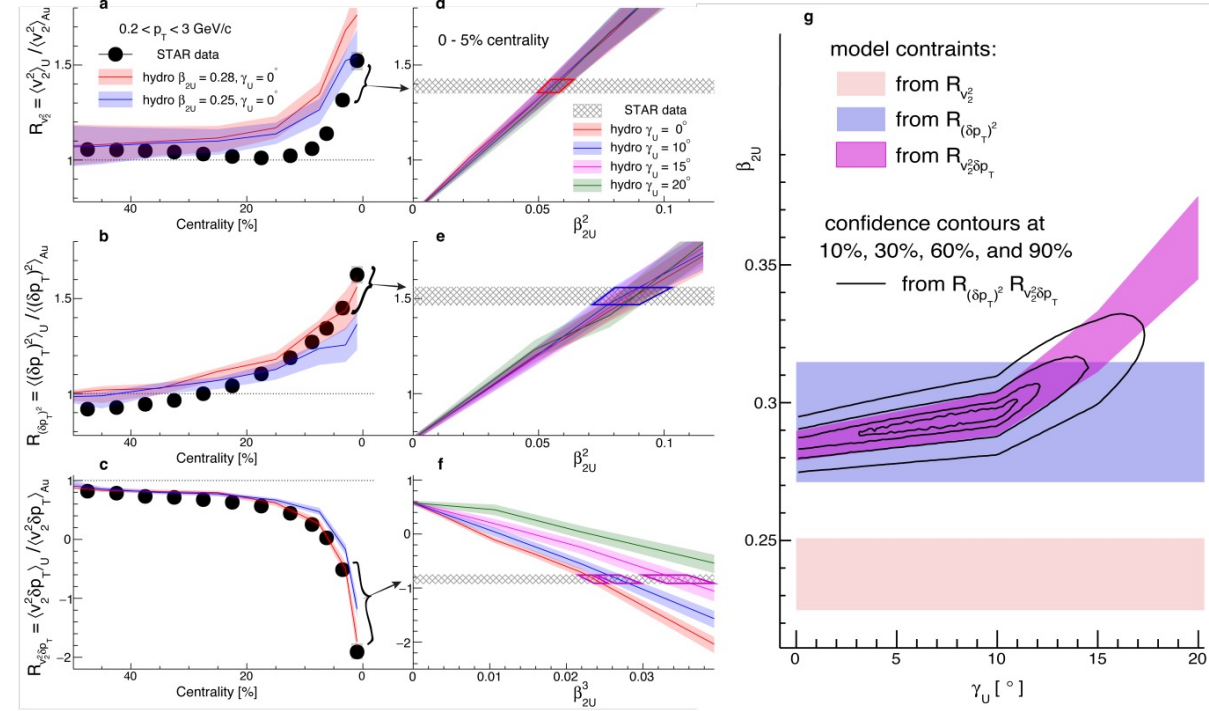
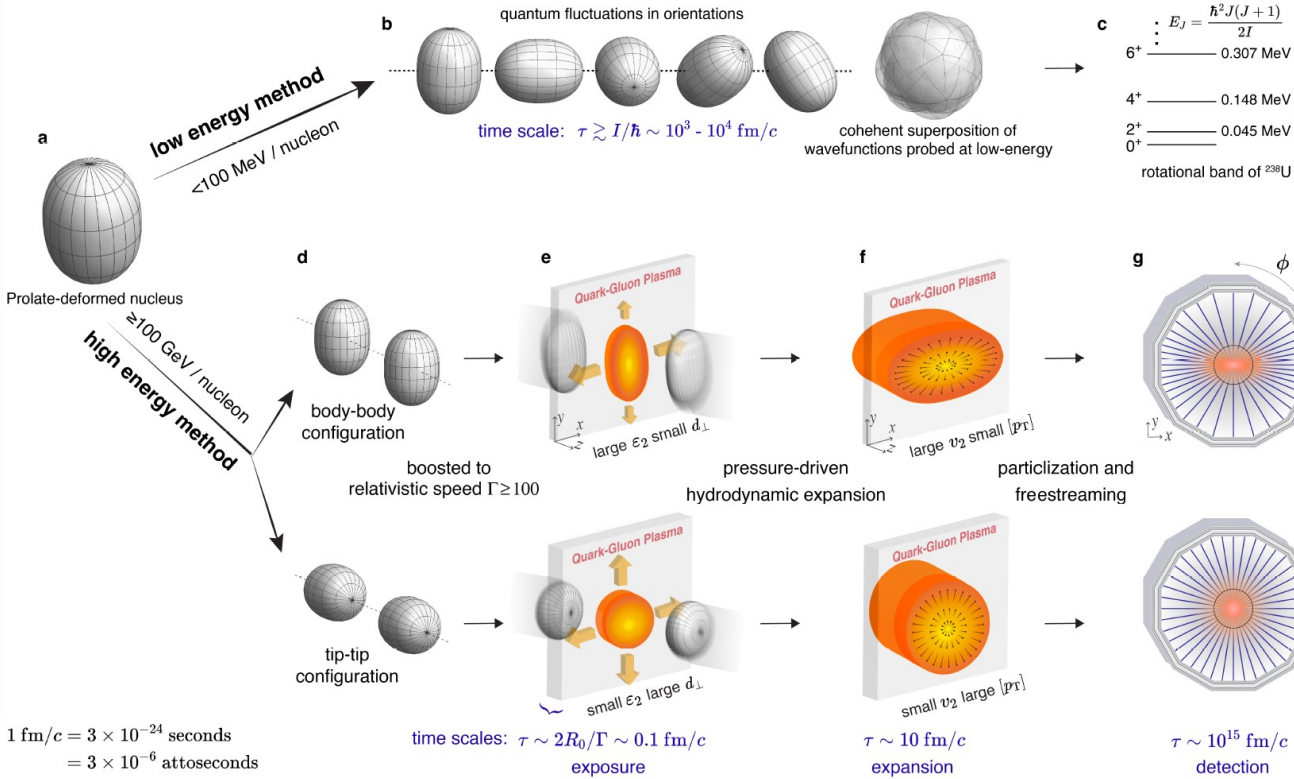


**Fig. 3 | Constraining the shape of  $^{238}\text{U}$ .** Left column: ratios of  $\langle v_2^2 \rangle$  (a),  $\langle (\delta p_T)^2 \rangle$  (b), and  $\langle v_2^2 \delta p_T \rangle$  (c) between U+U and Au+Au collisions as a function of centrality. The data are compared to the IP-Glasma+MUSIC hydrodynamic model calculation assuming  $\beta_{2U} = 0.28$  (red) and  $\beta_{2U} = 0.25$  (blue), whose shaded bands denote the

- This technique captures a collision-specific snapshot of the spatial matter distribution in the nuclei
- through the hydrodynamic expansion, leaves imprints on the particle momentum distribution
- U-238 an overall deformation broadly consistent, also a small deviation from axial symmetry
- Is nuclear structure at low energy directly applicable to gluon snapshot at high energy?

# Search for heavy antimatter and baryon objects

Rapid Communication

## Strangelet search

B. I. Abelev *et al.* (STAR Collab)  
Phys. Rev. C **76**, 011901(R) – Pu

**nature**

Explore content ▾ About the journal ▾ Publish with us ▾

nature > letters > article

Published: 24 April 2011

### Observation of the antimatter helium-4 nucleus

The STAR Collaboration

Nature **473**, 353–356 (2011) | [Cite this article](#)

**naturephysics**

Explore content ▾ About the journal ▾ Publish with us ▾

nature > nature physics > letters > article

Letter | Published: 09 March 2020

### Measurement of the mass difference and the binding energy of the hypertriton and antihypertriton

The STAR Collaboration

Nature Physics **16**, 409–412 (2020) | [Cite this article](#)

Science

Current Issue First release papers Archive

HOME > SCIENCE > VOL. 328, NO. 5974 > OBSERVATION OF AN ANTIMATTER HYPERNUCLEUS

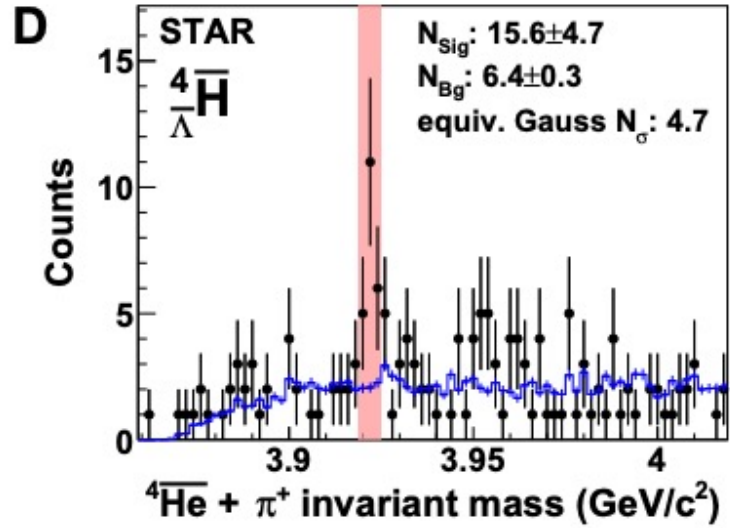
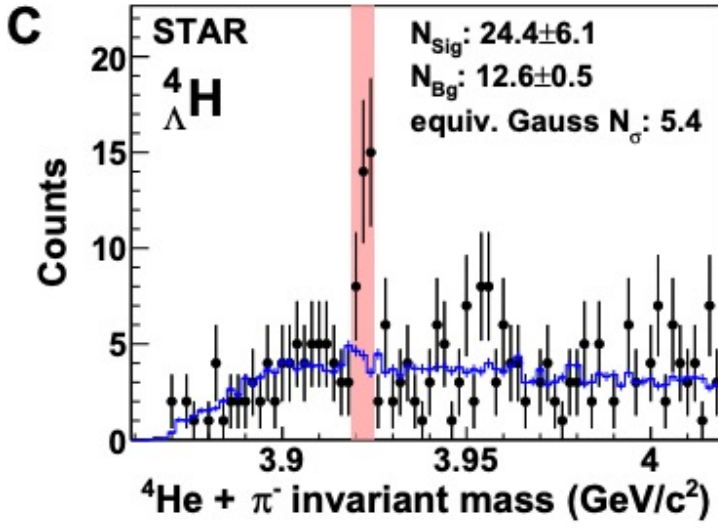
RESEARCH ARTICLE

## Observation of an Antimatter Hypernucleus

THE STAR COLLABORATION, B. I. ABELEV, M. M. AGGARWAL, Z. AHAMMED, A. V. ALAKHVERDYANTS, I. ALEKSEEV, B. D. ANDERSON, D. ARK

Y. ZOULKARNEEVA +382 authors [Authors Info & Affiliations](#)

SCIENCE • 4 Mar 2010 • Vol 328, Issue 5974 • pp. 58-62 • DOI: 10.1126/science.1183980



Submitted to Nature; arXiv:2310.12674



# Search for Stable Charmed Mesic Nucleus $D^-4\text{He}$ in Heavy-Ion and EIC

Possibility of Charmed Hypernuclei

C. B. Dover and S. H. Kahana  
Phys. Rev. Lett. **39**, 1506 – Published 12 December 1977

Zhangbu Xu (BNL)  
Cheng-Wei Lin, Yi Yang (NCKU)  
DNP (2022), EMMI (2023)

STAR@RHIC:

Estimate  $1 \times 10^5$ /year in forward acceptance  
But without vertex detector

EIC ion forward direction:

clean environment

Large boost factor for charm decay vertex

Nuclear cluster

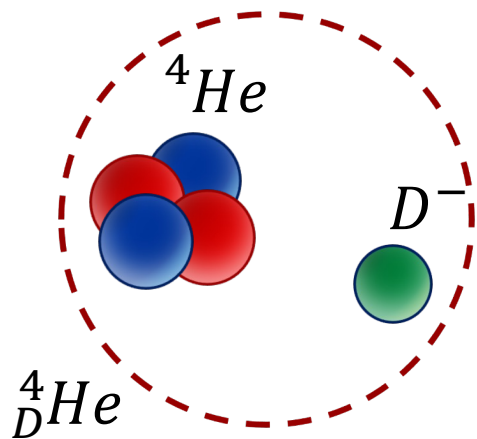
Article    References    Citing Articles (38)    PDF    Export Citation

>

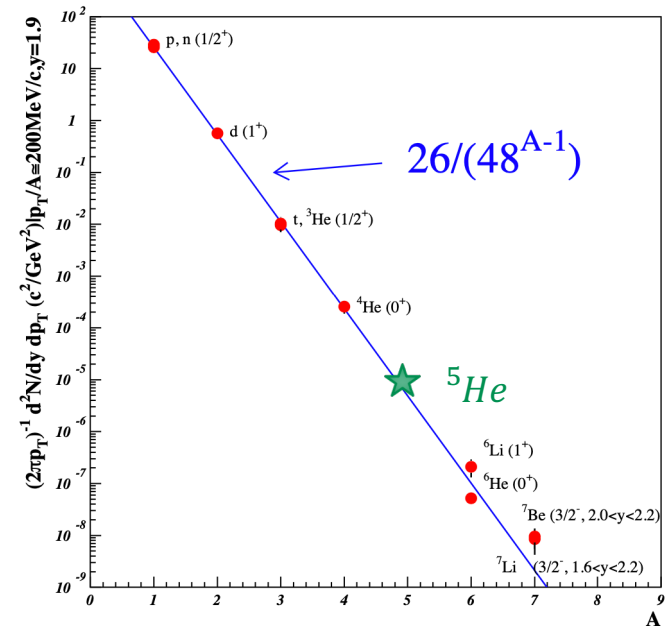
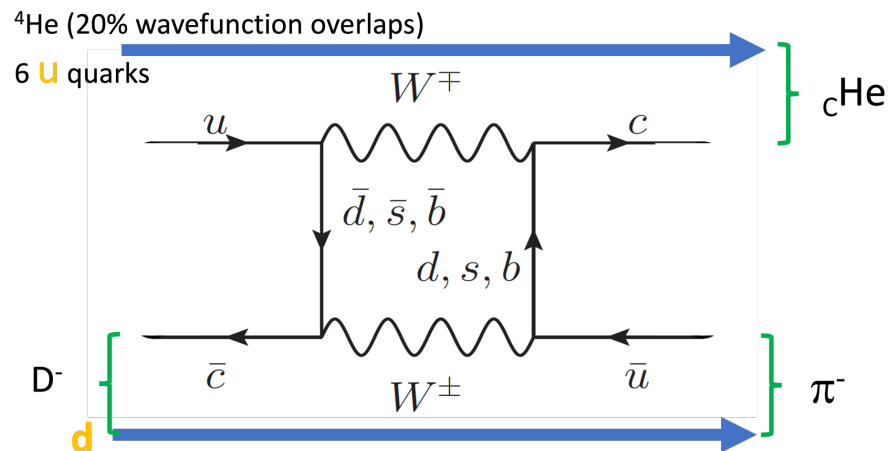
ABSTRACT

We suggest that both two-body and many-body bound states of a charmed baryon and nucleons should exist. Estimates indicate binding in the  $^1S_0$  state of  $C_1N$  ( $I = \frac{3}{2}$ ) and  $SN$  ( $I = 1$ ). We further estimate the binding energy of  $C_0, C_1$  in various finite nuclei.

Received 10 August 1977

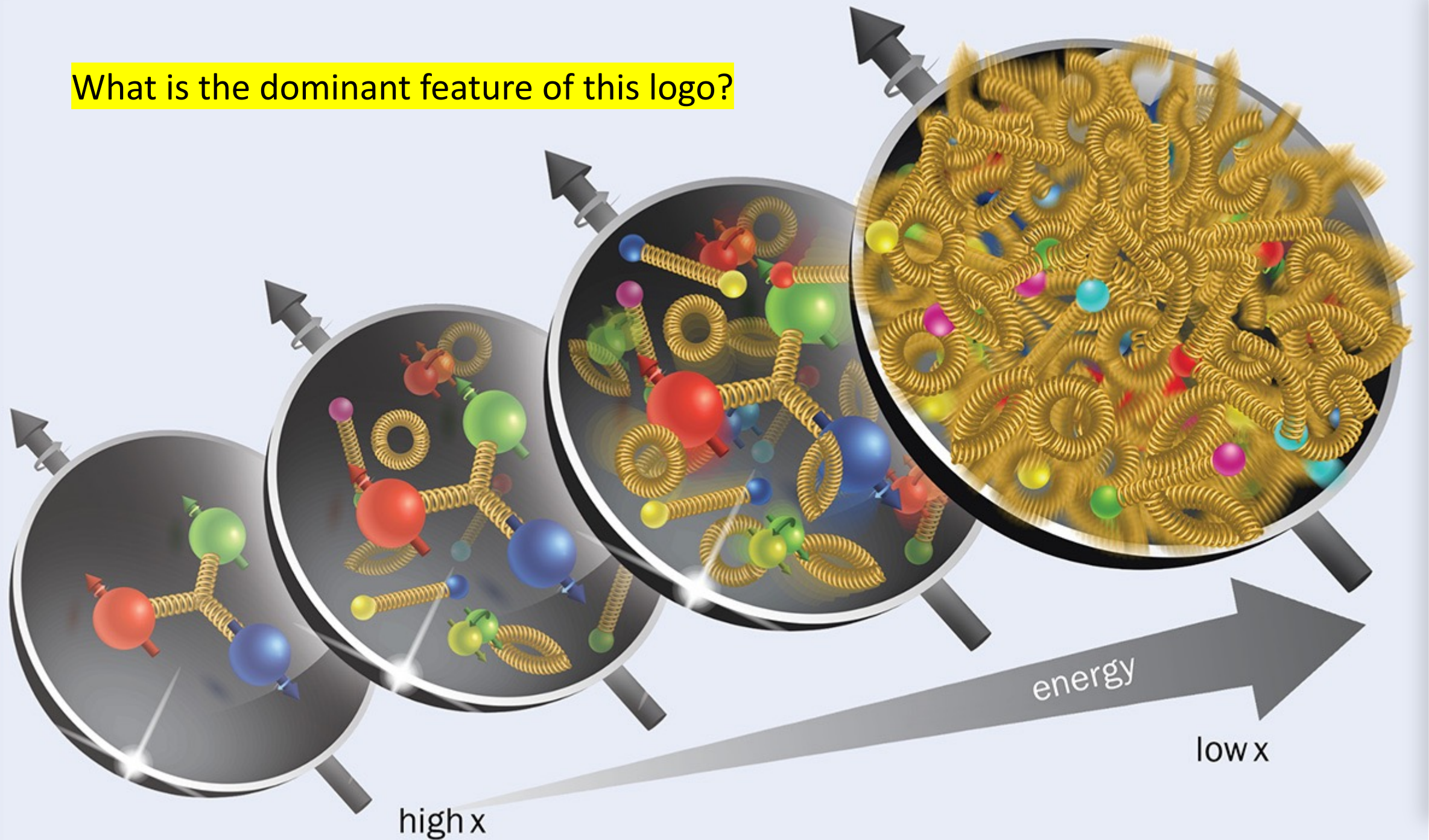


## Charm Quark Oscillation with large mass difference



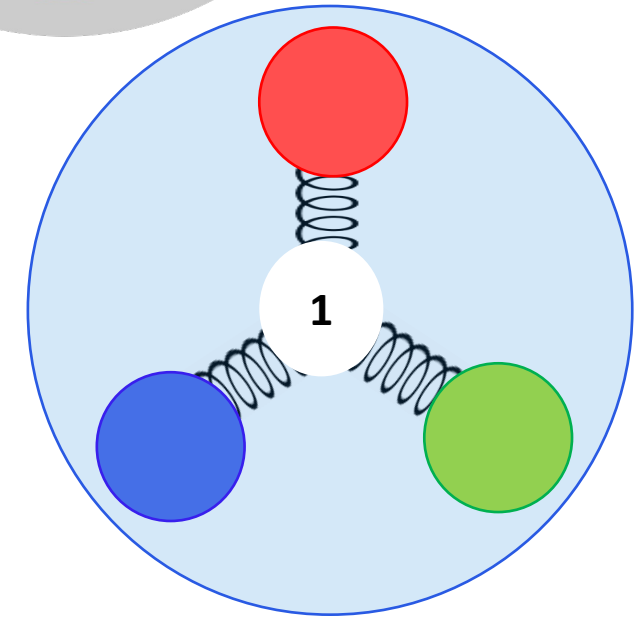
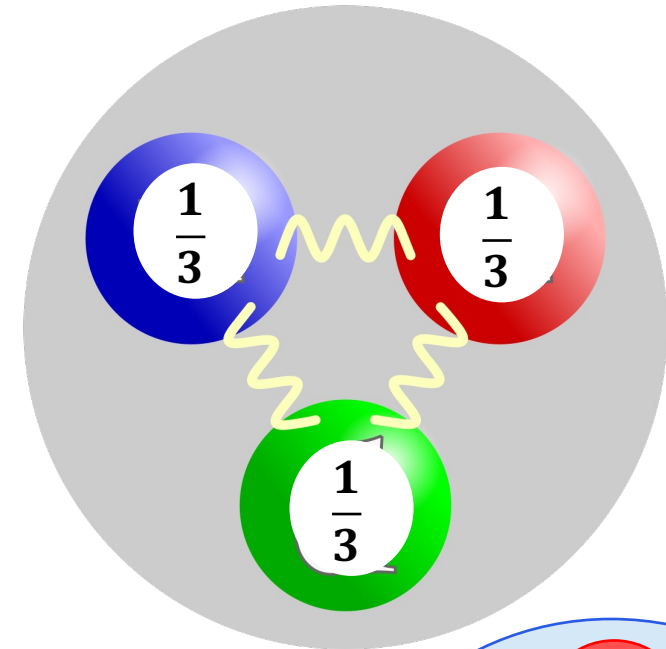
Phys. Rev. C **61**, 064908

What is the dominant feature of this logo?



# Baryon Number (B) Carrier

- Textbook picture of a proton
  - Lightest baryon with strictly conserved baryon number
  - Each valence quark carries  $\frac{1}{3}$  of baryon number
  - Proton lifetime  $>10^{34}$  years
  - Quarks are connected by gluons
- Alternative picture of a proton
  - Proposed at the Dawn of QCD in 1970s
  - A Y-shaped gluon junction topology carries baryon number ( $B=1$ )
  - The topology number is the strictly conserved number
  - Quarks do not carry baryon number
  - Valence quarks are connected to the end of the junction always
- **Neither of these postulations has been verified experimentally**



[1]: Artru, X.; String Model with Baryons: Topology, Classical Motion. Nucl. Phys. B 85, 442–460 (1975).

[2]: Rossi, G. C. & Veneziano, G. A; Possible Description of Baryon Dynamics in Dual and Gauge Theories. Nucl. Phys. B 123, 507–545 (1977)



## Can gluons trace baryon number?

D. Kharzeev

Theory Division, CERN, CH-1211 Geneva, Switzerland  
and Fakultät für Physik, Universität Bielefeld, D-33501 Bielefeld, Germany

Received 15 March 1996

Editor: R. Gatto

### Abstract

QCD as a gauge non-Abelian theory imposes severe constraints on the structure of the baryon wave function. We point out that, contrary to a widely accepted belief, the traces of baryon number in a high-energy process can reside in a non-perturbative configuration of gluon fields, rather than in the valence quarks. We argue that this conjecture can be tested experimentally, since it can lead to substantial baryon asymmetry in the central rapidity region of ultra-relativistic nucleus-nucleus collisions.

In QCD, quarks carry colour, flavour, electric charge and isospin. It seems only natural to assume that they also trace baryon number. However, this latter assumption is not dictated by the structure of QCD, and there-

**There is only one way to construct a gauge-invariant state vector of a baryon from quarks and gluons**

fore, the connection of the baryon number  $B = 1/3$  to quarks is based merely on the naive quark model classification. But any physical condition on the state vector should be satisfied by the state vector which is gauge-invariant – the constraint which is ignored in most of the naive quark model formulations. This constraint turns out to be very severe; in fact, there is only one way to construct a gauge-invariant state vector of a baryon from quarks and gluons [1] (note however that there is a large amount of freedom in choosing the paths connecting  $x$  to  $x_i$ ):

$$B = \epsilon^{ijk} \left[ P \exp \left( ig \int_{x_1}^x A_\mu dx^\mu \right) q(x_1) \right]_i \times \left[ P \exp \left( ig \int_{x_2}^x A_\mu dx^\mu \right) q(x_2) \right]_j$$

$$\times \left[ P \exp \left( ig \int_{x_3}^x A_\mu dx^\mu \right) q(x_3) \right]_k. \quad (1)$$

It is evident from the structure of (1) that the trace of baryon number should be associated not with the valence quarks, but with a non-perturbative configuration of gluon fields located at the point  $x$  – the “string junction” [1]. This can be nicely illustrated in the string picture: let us pull all of the quarks and

antiquarks to the point  $x$ . The tensor then constructs a local gauge-invariant state vector from the quark fields (see Fig. 1a). The  $B$  in Eq. (1) is a set of gauge invariant operators representing a baryon in QCD. With properly optimised parameters it is used extensively in the first principle computation of the nucleon mass. The purpose of this work is to study the non-nomological impact on baryon number production in the central region of nucleus-nucleus collisions.

It is evident from the structure of (1) that the trace of baryon number should be associated not with the valence quarks, but with a non-perturbative configuration of gluon fields located at the point  $x$  – the “string junction” [1]. This can be nicely illustrated in the string picture: let us pull all of the quarks and

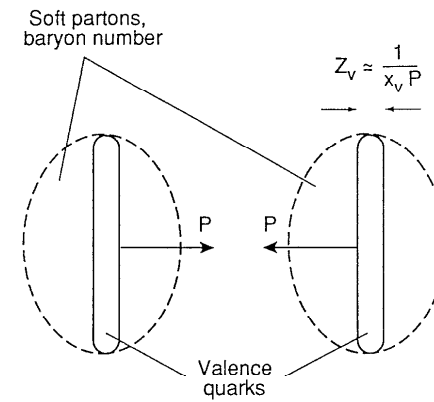


Fig. 2.

of the produced baryons will in general differ from the composition of colliding protons.

Why then is the leading baryon effect a gross feature of high-energy  $pp$  collisions? The reason may be the following. The string junction, connected to all three of the valence quarks, is confined inside the baryon, whereas  $pp$  collisions become on the average more and more peripheral at high energies. Therefore, in a typical high-energy collision, the string junctions of the colliding baryons pass far away from each other in the impact parameter plane and do not interact. One can however select only central events, triggering on high multiplicity of the produced hadrons. In this case, we expect that the string junctions will interact and may be stopped in the central rapidity region. This

**It is evident from the structure of (1) that the trace of baryon number should be associated not with the valence quarks, but with a non-perturbative configuration of gluon fields located at the point  $x$  – the “string junction”.**

[4]. These two observations combined indicate the existence of an appreciable baryon stopping in central  $pp$  collisions even at very high energies [3].

Where else do we encounter central baryon-baryon collisions? In a high energy nucleus-nucleus collision, the baryons in each of the colliding nuclei are densely packed in the impact parameter plane, with an average inter-baryon distance

$$r \simeq (\rho r_0)^{-1/2} A^{-1/6}, \quad (4)$$

where  $\rho$  is the nuclear density,  $r_0 \simeq 1.1$  fm, and  $A$  is the atomic number. The impact parameter  $b$  in an individual baryon-baryon interaction in the nucleus-nucleus collision is therefore effectively cut off by the packing parameter:  $b \leq r$ . In the case of a lead nucleus, for example,  $r$  appears to be very small:  $r \simeq 0.4$  fm, and a central lead-lead collision should therefore be accompanied by a large number of interactions among the string junctions. This may lead to substantial baryon stopping even at RHIC and LHC energies.

We shall now proceed to more quantitative considerations. In the topological expansion scheme [1], the separation of the baryon number flow from the flow of valence quarks in baryon-(anti)baryon interaction can be represented through a  $t$ -channel exchange of the quarkless junction-antijunction state with the wave function given by

$$M_0^j = \epsilon_{ijk} \epsilon^{i'j'k'} \left[ P \exp \left( ig \int_{x_1}^{x_2} A_\mu dx^\mu \right) \right]_{i'}^i \times \left[ P \exp \left( ig \int_{x_1}^{x_2} A_\mu dx^\mu \right) \right]_{j'}^j \times \left[ P \exp \left( ig \int_{x_1}^{x_2} A_\mu dx^\mu \right) \right]_{k'}^k. \quad (5)$$

The structure of the wave function (5) is illustrated in Fig. 1b – it is a quarkless closed string configuration composed from a junction and an antijunction. In the topological expansion scheme, the states (5) lie on a Regge trajectory; its intercept can be related to the baryon and reggeon intercepts [1]:

$$\alpha_0^j(0) \simeq 2\alpha_B(0) - 1 + 3(1 - \alpha_R(0)) \simeq \frac{1}{2}, \quad (6)$$

## Can gluons trace baryon number?

D. Kharzeev

Theory Division, CERN, CH-1211 Geneva, Switzerland  
and Fakultät für Physik, Universität Bielefeld, D-33501 Bielefeld, Germany

Received 15 March 1996  
Editor: R. Gatto

### Abstract

QCD as a gauge non-Abelian theory imposes severe constraints on the structure of the baryon wave function. We point out that, contrary to a widely accepted belief, the traces of baryon number in a high-energy process can reside in a non-perturbative configuration of gluon fields, rather than in the valence quarks. We argue that this conjecture can be tested experimentally, since it can lead to substantial baryon asymmetry in the central rapidity region of ultra-relativistic nucleus-nucleus collisions.

In QCD, quarks carry colour, flavour, electric charge and isospin. It seems only natural to assume that they also trace baryon number. However, this latter assumption is not dictated by the structure of QCD, and there-

**There is only one way to construct a gauge-invariant state vector of a baryon from quarks and gluons**

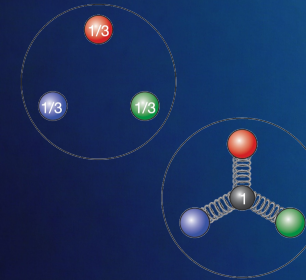
$$\times \left[ P \exp \left( ig \int_{x_3}^x A_\mu dx^\mu \right) q(x_3) \right]_k \quad (1)$$

is not dictated by the structure of QCD, and there-  
fore, it is not clear how to construct a gauge-invariant  
state vector of a baryon from quarks and gluons.  
But any physical state vector should be gauge-invariant.  
The constraint which is ignored in most of the naive quark model  
formulations. This constraint turns out to be very severe;  
in fact, there is only one way to construct a gauge-  
invariant state vector of a baryon from quarks and glu-  
ons [1] (note however that there is a large amount of  
freedom in choosing the paths connecting  $x$  to  $x_i$ ):

$$B = \epsilon^{ijk} \left[ P \exp \left( ig \int_{x_1}^x A_\mu dx^\mu \right) q(x_1) \right]_i \\ \times \left[ P \exp \left( ig \int_{x_2}^x A_\mu dx^\mu \right) q(x_2) \right]_j$$

It is evident from the structure of (1) that the trace of baryon number should be associated not with the valence quarks, but with a non-perturbative configuration of gluon fields located at the point  $x$  - the “string junction” [1]. This can be nicely illustrated in the string picture: let us pull all of the quarks away from the point  $x$  - the “st-

# FIRST WORKSHOP ON BARYON DYNAMICS FROM RHIC TO EIC



Dates: Jan 22 – 24, 2024

Location: Center for Frontiers in Nuclear Science (CFNS), Stony Brook University

Format: In-person & zoom

Participation: Invited Talks + Open Mic Discussion

Registration Deadline: Jan 15th, 2024

No registration fee - Limited student support available

### Scientific Motivation:

This workshop aims to address fundamental questions such as what carries the baryon quantum number and how a baryon is stopped in high-energy collisions, which have profound implications for understanding the baryon structure. It also challenges our current knowledge of QCD and its non-perturbative aspects, such as baryon junctions and gluonic topology. The workshop will explore the origin and transport of baryons in high-energy collisions, from the AGS/SPS/RHIC/LHC to JLab  $F_{\pi}$ , HERA/EIC, and discuss the experimental and theoretical challenges and opportunities in this field.

### Key Topics:

- Baryon junctions and gluonic topology
- Baryon and charge stopping in heavy-ion collisions
- Baryon transport in photon-induced processes
- Baryon-meson-transition in backward u-channel reaction
- Models of baryon dynamics and baryon-rich matter
- Novel experimental methods at EIC

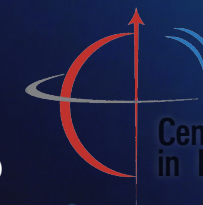
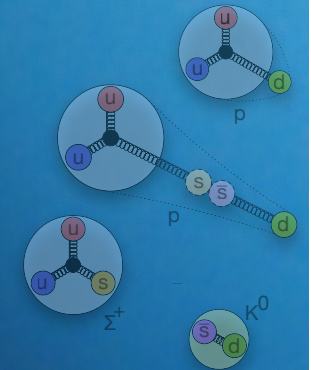
Keynote speaker: Gabriele Veneziano

### Organizers:

- D. Kharzeev (SBU/BNL)
- W. B. Li (SBU/CFNS)
- N. Lewis (Rice)
- J. Noronha Hostlar (UIUC)
- C. Shen (Wayne State/RBRC)
- P. Tribedy (BNL)
- Z. Xu (BNL)

Webpage: <https://indico.cfnsbu.physics.sunysb.edu/event/113/>

Contact: [ptribedy@bnl.gov](mailto:ptribedy@bnl.gov)



Center for Frontiers  
in Nuclear Science



Stony Brook  
University

# Three approaches toward tracking the origin of the baryon number

## 1. STAR Method:

Charge (Q) stopping vs baryon (B) stopping:  
if valence quarks carry Q and B,  
Q=B at middle rapidity

$$B/Q=2$$

## 2. Kharzeev-STAR Method:

If gluon topology (J) carries B as one unit,  
it should show scaling according to

Regge theory

$$\alpha_B=0.61$$

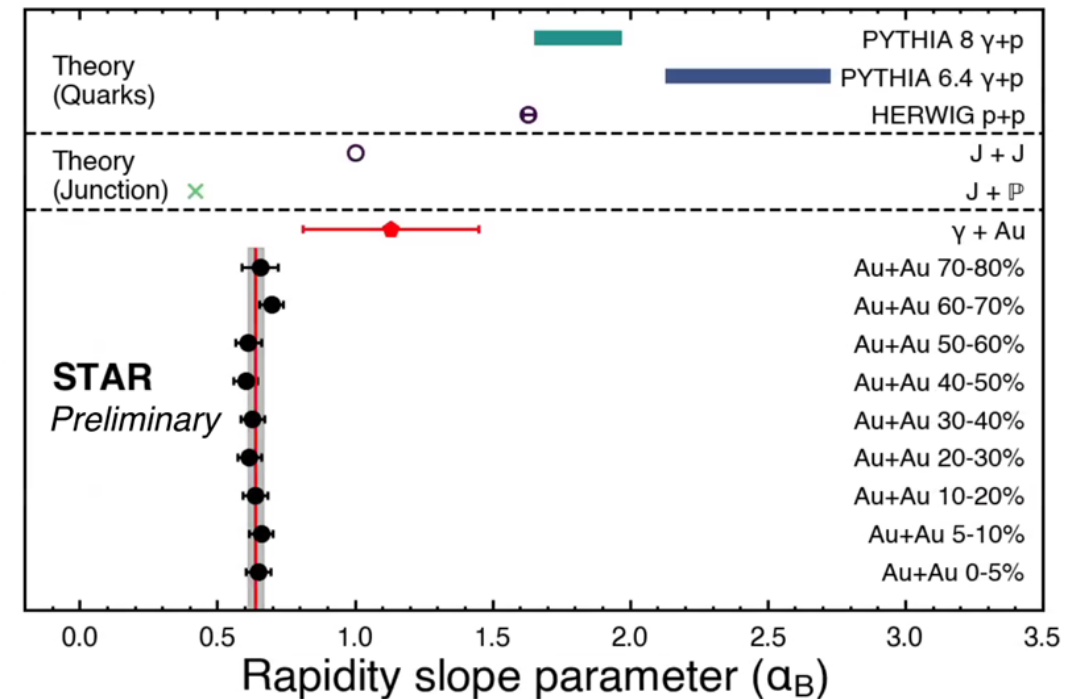
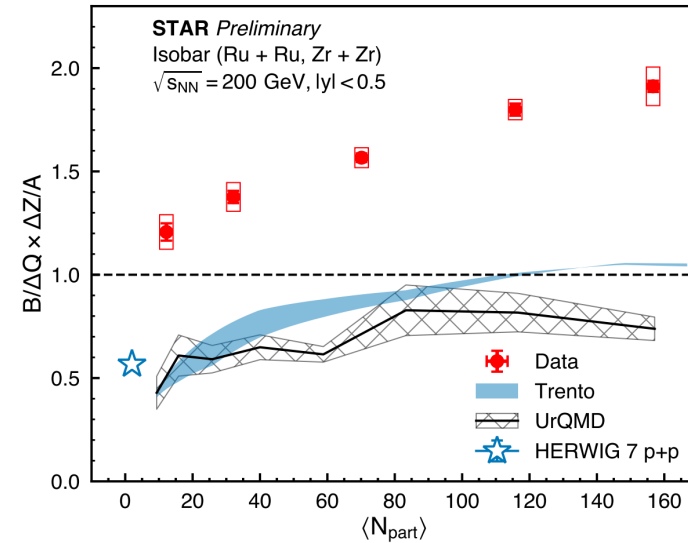
$$p = \sim e^{-\alpha_B y}$$

$$\alpha_B \sim 0.5$$

## 3. Artru Method:

In  $\gamma$ +Au collision, rapidity asymmetry can  
reveal the origin

$$\alpha_B(A+A)=0.61 < \alpha_B(\gamma+A)=1.1 < \alpha_B(\text{PYTHIA})$$





# EIC simulation of baryon vs charge transports

Summary of the 1<sup>st</sup> workshop on 2<sup>nd</sup> EIC detector (05/15/23)

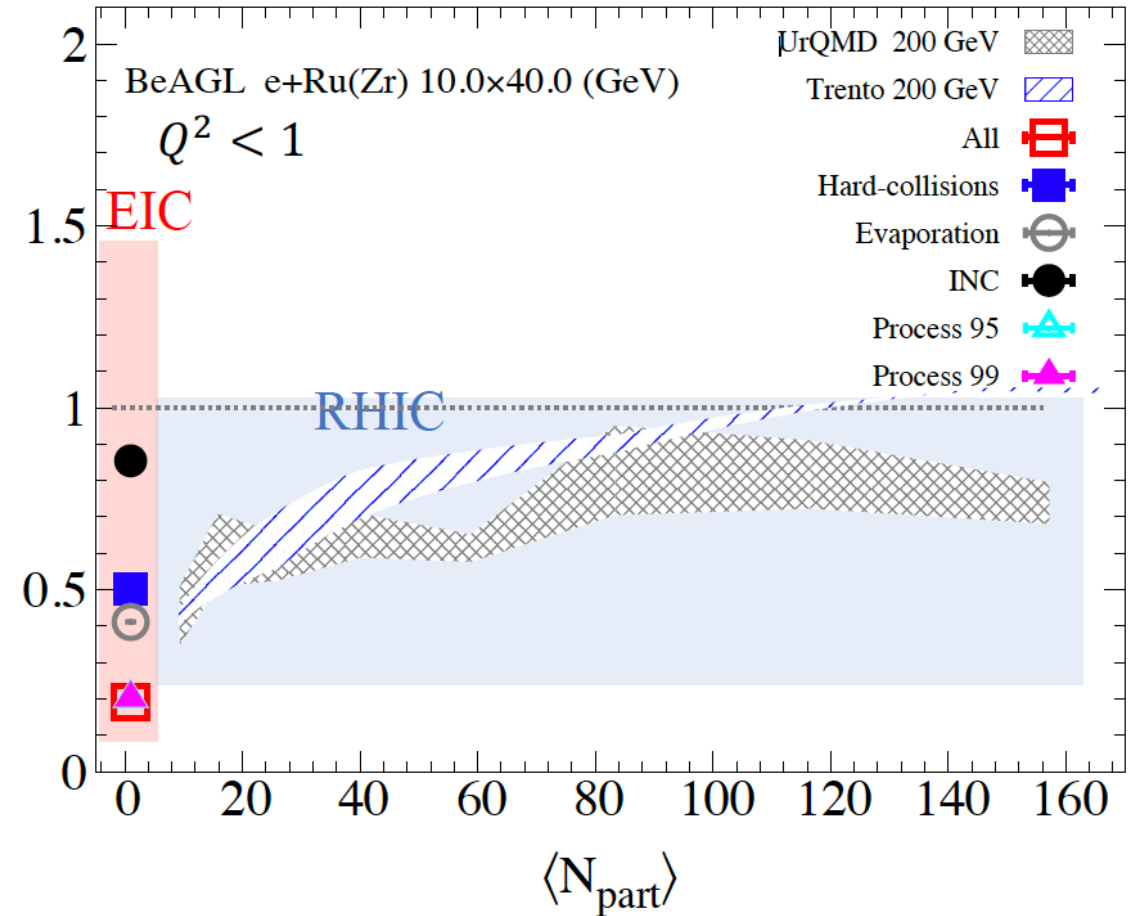
## Golden Channels Strawman

CHANNEL	PHYSICS	DETECTOR II OPPORTUNITY
Diffractive dijet	Wigner Distribution	detection of forward scattered proton/nucleus + detection of low $p_T$ particles
DVCS on nuclei	Nuclear GPDs	High resolution photon + detection of forward scattered proton/nucleus
Baryon/Charge Stopping	Origin of Baryon # in QCD	PID and detection for low $p_T$ $\pi/K/p$
$F_2$ at low $x$ and $Q^2$	Probes transition from partonic to color dipole regime	Maximize $Q^2$ tagger down to 0.1 GeV and integrate into IR.
Coherent VM Production	Nuclear shadowing and saturation	High resolution tracking for precision $t$ reconstruction

These channels are just a starting point, a way to initially focus activities within the group. Additional ideas and efforts are welcome!

- Need small  $Q^2$ , large rapidity coverage and low-momentum hadron particle identification  
 $Q^2 \leq 1 \text{ GeV}^2$ ;  $\pi/k/p$  PID  $p_t \geq \sim 100 \text{ MeV}$
- Isobar collisions to measure charge transport (quark transports), Zr/Ru;  $^7\text{Li}/^7\text{Be}$

Niseem Magdy (SBU)



EIC can measure the baryon junction distribution function

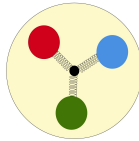
## Introduction: baryon junctions

It has been suggested [1] that baryon number is carried by a gluonic string junction. It ensures gauge invariance of the operator containing three quark fields at different points.

Gauge-invariant baryon operator:

$$B(x_1, x_2, x_3) \sim \eta(x_1)\eta(x_2)\eta(x_3) \xrightarrow{\text{Gauge inv.}} B(x_1, x_2, x_3, x) = e^{i\chi} [P \exp(i\int_{x_1}^x A_\mu dx^\mu)\eta(x_1)] [P \exp(i\int_{x_2}^x A_\mu dx^\mu)\eta(x_2)] [P \exp(i\int_{x_3}^x A_\mu dx^\mu)\eta(x_3)]$$

If a string breaks, the baryon is restored around the junction. Does the junction carry the baryon number?



A schematic illustration of the baryon junction structure



### (1+1)-dimensional QCD

QCD in (1+1) is similar to (3+1): confinement, chiral symmetry breaking and mass gap in meson

and baryon spectrum and is exactly solvable in the large  $N_c$  limit.

Bosonization → sine-Gordon model:

$$\mathcal{L} = \frac{1}{2}(\partial_t \phi)^2 - m^2 \cos\left(2\sqrt{\frac{\pi}{N_c}}\phi\right)$$

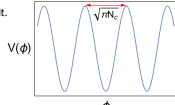


Fig. 1 Potential of the sine-Gordon field

Baryon is represented by a topological kink (see Figure 2).

Baryon number is naturally topological charge.

Quantum state of a baryon is a particular coherent state [2]:

$$|B\rangle = \bigotimes_k |\alpha_k\rangle, \quad |\alpha_k\rangle = e^{-|\alpha_k|^2/2} \sum_{n=0}^{\infty} \frac{\alpha_k^n}{n!} (a_k^\dagger)^n |0\rangle$$

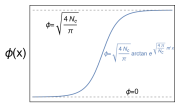


Fig. 2 Sine-Gordon kink field profile

where  $a_k^\dagger$  create soliton constituents, not free quanta.

$\alpha_k$  are Fourier coefficients of the classical kink profile:

$$\alpha_k = t_k c_k, \quad t_k = -\frac{i}{2k}, \quad c_k = \sqrt{2\sqrt{2\pi N_c} |k|} \frac{1}{\cosh\left(\sqrt{\frac{2\pi}{N_c}} \frac{2kx}{2\omega}\right)}$$

leading to a natural decomposition of the coherent state into topology and "energy":

$$|\alpha_k\rangle = e^{-\frac{1}{2}|\alpha_k|^2} \sum_{n_k=0}^{\infty} \frac{t_k^{n_k} c_k^{n_k}}{\sqrt{n_k!}} |n_k\rangle_t \otimes |n_k\rangle_e$$

Reduced density matrix after tracing over the topological degrees of freedom:

$$\rho_{red} = \bigotimes_k \rho_k = \bigotimes_k \sum_{n_k=0}^{\infty} \frac{|\alpha_k|^{2n_k}}{n_k!} |n_k\rangle_e \langle n_k|_e$$

Compute the entanglement entropy:

$$S_k = -\text{Tr}(\rho_k \log \rho_k) = |\alpha_k|^2 (1 - \log |\alpha_k|^2) + e^{-|\alpha_k|^2} \sum_{n=2}^{\infty} |\alpha_k|^{2n} \frac{\log n!}{n!}$$

Estimate the asymptotic behavior at small and large  $k$  analytically; the rest can be computed numerically. Results are shown on Fig. 3

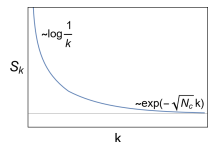


Fig. 3 Entanglement entropy as a function of momentum. Most entanglement is concentrated near zero momentum which corresponds to small  $x$ .

• We find entanglement between topological degrees of freedom (carrying the baryon number) and the rest of the baryon wavefunction.

• Entanglement is strongly enhanced at small momentum (fraction).

• Flavor-independent forward baryon production rate since no valence quarks remain with the junction

• Large flavor-independent meson multiplicity

• Characteristic rapidity dependence (see Figure 7), decreasing in the forward direction slower than naively expected

•  $M_0^+$  has the largest intercept so the corresponding process dominates at large  $s$ .

• Rapidity dependence estimated (see Fig. 7)

• Flavor-independent forward baryon production rate since no valence quarks remain with the junction

• Large flavor-independent meson multiplicity

• Characteristic rapidity dependence (see Figure 7), decreasing in the forward direction slower than naively expected

•  $M_0^+$  has the largest intercept so the corresponding process dominates at large  $s$ .

• Rapidity dependence estimated (see Fig. 7)

• Flavor-independent forward baryon production rate since no valence quarks remain with the junction

• Large flavor-independent meson multiplicity

• Characteristic rapidity dependence (see Figure 7), decreasing in the forward direction slower than naively expected

•  $M_0^+$  has the largest intercept so the corresponding process dominates at large  $s$ .

• Rapidity dependence estimated (see Fig. 7)

• Flavor-independent forward baryon production rate since no valence quarks remain with the junction

• Large flavor-independent meson multiplicity

• Characteristic rapidity dependence (see Figure 7), decreasing in the forward direction slower than naively expected

•  $M_0^+$  has the largest intercept so the corresponding process dominates at large  $s$ .

• Rapidity dependence estimated (see Fig. 7)

• Flavor-independent forward baryon production rate since no valence quarks remain with the junction

• Large flavor-independent meson multiplicity

• Characteristic rapidity dependence (see Figure 7), decreasing in the forward direction slower than naively expected

•  $M_0^+$  has the largest intercept so the corresponding process dominates at large  $s$ .

• Rapidity dependence estimated (see Fig. 7)

• Flavor-independent forward baryon production rate since no valence quarks remain with the junction

• Large flavor-independent meson multiplicity

• Characteristic rapidity dependence (see Figure 7), decreasing in the forward direction slower than naively expected

•  $M_0^+$  has the largest intercept so the corresponding process dominates at large  $s$ .

• Rapidity dependence estimated (see Fig. 7)

• Flavor-independent forward baryon production rate since no valence quarks remain with the junction

• Large flavor-independent meson multiplicity

• Characteristic rapidity dependence (see Figure 7), decreasing in the forward direction slower than naively expected

•  $M_0^+$  has the largest intercept so the corresponding process dominates at large  $s$ .

• Rapidity dependence estimated (see Fig. 7)

• Flavor-independent forward baryon production rate since no valence quarks remain with the junction

• Large flavor-independent meson multiplicity

• Characteristic rapidity dependence (see Figure 7), decreasing in the forward direction slower than naively expected

•  $M_0^+$  has the largest intercept so the corresponding process dominates at large  $s$ .

• Rapidity dependence estimated (see Fig. 7)

• Flavor-independent forward baryon production rate since no valence quarks remain with the junction

• Large flavor-independent meson multiplicity

• Characteristic rapidity dependence (see Figure 7), decreasing in the forward direction slower than naively expected

•  $M_0^+$  has the largest intercept so the corresponding process dominates at large  $s$ .

• Rapidity dependence estimated (see Fig. 7)

• Flavor-independent forward baryon production rate since no valence quarks remain with the junction

• Large flavor-independent meson multiplicity

• Characteristic rapidity dependence (see Figure 7), decreasing in the forward direction slower than naively expected

•  $M_0^+$  has the largest intercept so the corresponding process dominates at large  $s$ .

• Rapidity dependence estimated (see Fig. 7)

• Flavor-independent forward baryon production rate since no valence quarks remain with the junction

• Large flavor-independent meson multiplicity

• Characteristic rapidity dependence (see Figure 7), decreasing in the forward direction slower than naively expected

•  $M_0^+$  has the largest intercept so the corresponding process dominates at large  $s$ .

• Rapidity dependence estimated (see Fig. 7)

• Flavor-independent forward baryon production rate since no valence quarks remain with the junction

• Large flavor-independent meson multiplicity

• Characteristic rapidity dependence (see Figure 7), decreasing in the forward direction slower than naively expected

•  $M_0^+$  has the largest intercept so the corresponding process dominates at large  $s$ .

• Rapidity dependence estimated (see Fig. 7)

• Flavor-independent forward baryon production rate since no valence quarks remain with the junction

• Large flavor-independent meson multiplicity

• Characteristic rapidity dependence (see Figure 7), decreasing in the forward direction slower than naively expected

•  $M_0^+$  has the largest intercept so the corresponding process dominates at large  $s$ .

• Rapidity dependence estimated (see Fig. 7)

• Flavor-independent forward baryon production rate since no valence quarks remain with the junction

• Large flavor-independent meson multiplicity

• Characteristic rapidity dependence (see Figure 7), decreasing in the forward direction slower than naively expected

•  $M_0^+$  has the largest intercept so the corresponding process dominates at large  $s$ .

• Rapidity dependence estimated (see Fig. 7)

• Flavor-independent forward baryon production rate since no valence quarks remain with the junction

• Large flavor-independent meson multiplicity

• Characteristic rapidity dependence (see Figure 7), decreasing in the forward direction slower than naively expected

•  $M_0^+$  has the largest intercept so the corresponding process dominates at large  $s$ .

• Rapidity dependence estimated (see Fig. 7)

• Flavor-independent forward baryon production rate since no valence quarks remain with the junction

• Large flavor-independent meson multiplicity

• Characteristic rapidity dependence (see Figure 7), decreasing in the forward direction slower than naively expected

•  $M_0^+$  has the largest intercept so the corresponding process dominates at large  $s$ .

• Rapidity dependence estimated (see Fig. 7)

• Flavor-independent forward baryon production rate since no valence quarks remain with the junction

• Large flavor-independent meson multiplicity

• Characteristic rapidity dependence (see Figure 7), decreasing in the forward direction slower than naively expected

•  $M_0^+$  has the largest intercept so the corresponding process dominates at large  $s$ .

• Rapidity dependence estimated (see Fig. 7)

• Flavor-independent forward baryon production rate since no valence quarks remain with the junction

• Large flavor-independent meson multiplicity

• Characteristic rapidity dependence (see Figure 7), decreasing in the forward direction slower than naively expected

•  $M_0^+$  has the largest intercept so the corresponding process dominates at large  $s$ .

• Rapidity dependence estimated (see Fig. 7)

• Flavor-independent forward baryon production rate since no valence quarks remain with the junction

• Large flavor-independent meson multiplicity

• Characteristic rapidity dependence (see Figure 7), decreasing in the forward direction slower than naively expected

•  $M_0^+$  has the largest intercept so the corresponding process dominates at large  $s$ .

• Rapidity dependence estimated (see Fig. 7)

• Flavor-independent forward baryon production rate since no valence quarks remain with the junction

• Large flavor-independent meson multiplicity

• Characteristic rapidity dependence (see Figure 7), decreasing in the forward direction slower than naively expected

•  $M_0^+$  has the largest intercept so the corresponding process dominates at large  $s$ .

• Rapidity dependence estimated (see Fig. 7)

• Flavor-independent forward baryon production rate since no valence quarks remain with the junction

• Large flavor-independent meson multiplicity

• Characteristic rapidity dependence (see Figure 7), decreasing in the forward direction slower than naively expected

•  $M_0^+$  has the largest intercept so the corresponding process dominates at large  $s$ .

• Rapidity dependence estimated (see Fig. 7)

• Flavor-independent forward baryon production rate since no valence quarks remain with the junction

• Large flavor-independent meson multiplicity

• Characteristic rapidity dependence (see Figure 7), decreasing in the forward direction slower than naively expected

•  $M_0^+$  has the largest intercept so the corresponding process dominates at large  $s$ .

• Rapidity dependence estimated (see Fig. 7)

• Flavor-independent forward baryon production rate since no valence quarks remain with the junction

• Large flavor-independent meson multiplicity

• Characteristic rapidity dependence (see Figure 7), decreasing in the forward direction slower than naively expected

•  $M_0^+$  has the largest intercept so the corresponding process dominates at large  $s$ .

• Rapidity dependence estimated (see Fig. 7)

• Flavor-independent forward baryon production rate since no valence quarks remain with the junction

• Large flavor-independent meson multiplicity

• Characteristic rapidity dependence (see Figure 7), decreasing in the forward direction slower than naively expected

•  $M_0^+$  has the largest intercept so the corresponding process dominates at large  $s$ .

• Rapidity dependence estimated (see Fig. 7)

• Flavor-independent forward baryon production rate since no valence quarks remain with the junction

• Large flavor-independent meson multiplicity

• Characteristic rapidity dependence (see Figure 7), decreasing in the forward direction slower than naively expected

•  $M_0^+$  has the largest intercept so the corresponding process dominates at large  $s$ .

• Rapidity dependence estimated (see Fig. 7)

• Flavor-independent forward baryon production rate since no valence quarks remain with the junction

• Large flavor-independent meson multiplicity

• Characteristic rapidity dependence (see Figure 7), decreasing in the forward direction slower than naively expected

•  $M_0^+$  has the largest intercept so the corresponding process dominates at large  $s$ .

• Rapidity dependence estimated (see Fig. 7)

• Flavor-independent forward baryon production rate since no valence quarks remain with the junction

• Large flavor-independent meson multiplicity

• Characteristic rapidity dependence (see Figure 7), decreasing in the forward direction slower than naively expected

•  $M_0^+$  has the largest intercept so the corresponding process dominates at large  $s$ .

• Rapidity dependence estimated (see Fig. 7)

• Flavor-independent forward baryon production rate since no valence quarks remain with the junction

• Large flavor-independent meson multiplicity

• Characteristic rapidity dependence (see Figure 7), decreasing in the forward direction slower than naively expected

•  $M_0^+$  has the largest intercept so the corresponding process dominates at large  $s$ .

• Rapidity dependence estimated (see Fig. 7)

• Flavor-independent forward baryon production rate since no valence quarks remain with the junction

• Large flavor-independent meson multiplicity

• Characteristic rapidity dependence (see Figure 7), decreasing in the forward direction slower than naively expected

•  $M_0^+$  has the largest intercept so the corresponding process dominates at large  $s$ .

• Rapidity dependence estimated (see Fig. 7)

• Flavor-independent forward baryon production rate since no valence quarks remain with the junction

• Large flavor-independent meson multiplicity

• Characteristic rapidity dependence (see Figure 7), decreasing in the forward direction slower than naively expected

•  $M_0^+$  has the largest intercept so the corresponding process dominates at large  $s$ .

• Rapidity dependence estimated (see Fig. 7)

• Flavor-independent forward baryon production rate since no valence quarks remain with the junction

• Large flavor-independent meson multiplicity

• Characteristic rapidity dependence (see Figure 7), decreasing in the forward direction slower than naively expected

•  $M_0^+$  has the largest intercept so the corresponding process dominates at large  $s$ .

• Rapidity dependence estimated (see Fig. 7)

• Flavor-independent forward baryon production rate since no valence quarks remain with the junction

• Large flavor-independent meson multiplicity

• Characteristic rapidity dependence (see Figure 7), decreasing in the forward direction slower than naively expected

•  $M_0^+$  has the largest intercept so the corresponding process dominates at large  $s$ .

• Rapidity dependence estimated (see Fig. 7)

• Flavor-independent forward baryon production rate since no valence quarks remain with the junction

• Large flavor-independent meson multiplicity

• Characteristic rapidity dependence (see Figure 7), decreasing in the forward direction slower than naively expected

•  $M_0^+$  has the largest intercept so the corresponding process dominates at large  $s$ .

• Rapidity dependence estimated (see Fig. 7)

• Flavor-independent forward baryon production rate since no valence quarks remain with the junction

• Large flavor-independent meson multiplicity

• Characteristic rapidity dependence (see Figure 7), decreasing in the forward direction slower than naively expected

•  $M_0^+$  has the largest intercept so the corresponding process dominates at large  $s$ .

• Rapidity dependence estimated (see Fig. 7)

• Flavor-independent forward baryon production rate since no valence quarks remain with the junction

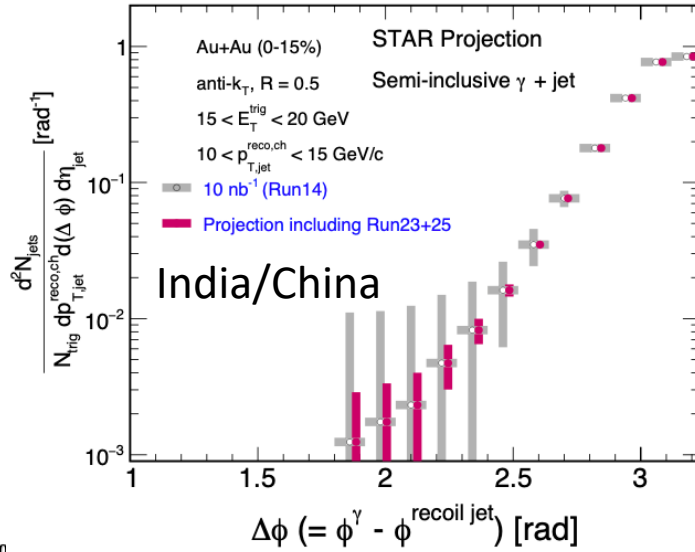
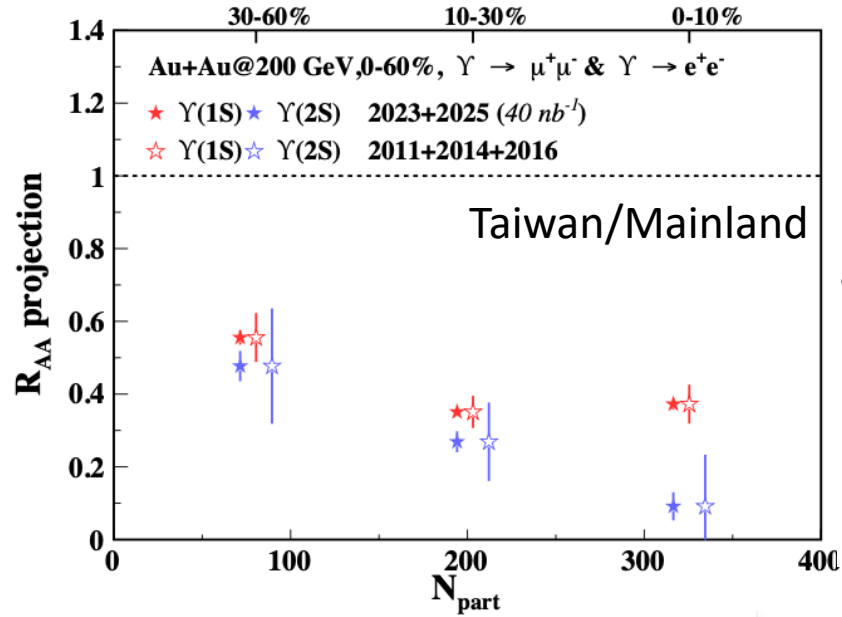
• Large flavor-independent meson multiplicity

• Characteristic rapidity dependence (see Figure 7), decreasing in the forward direction slower than naively expected

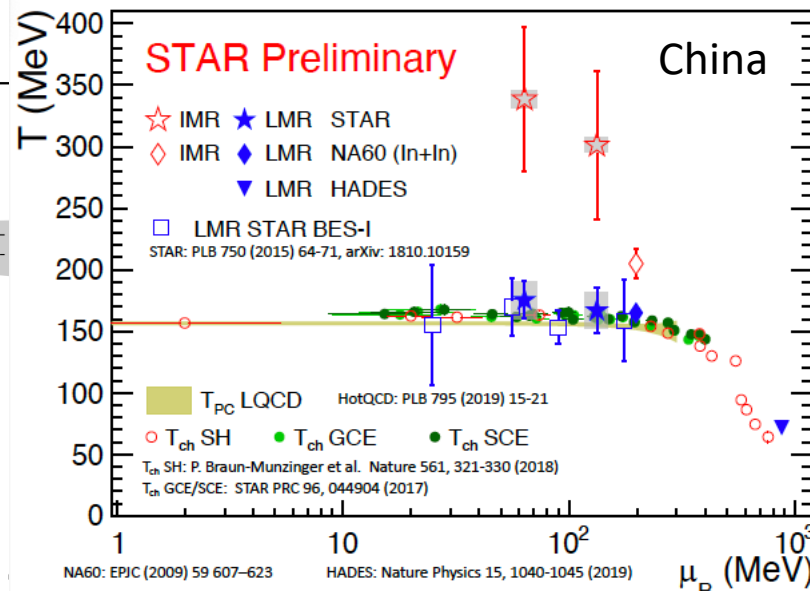
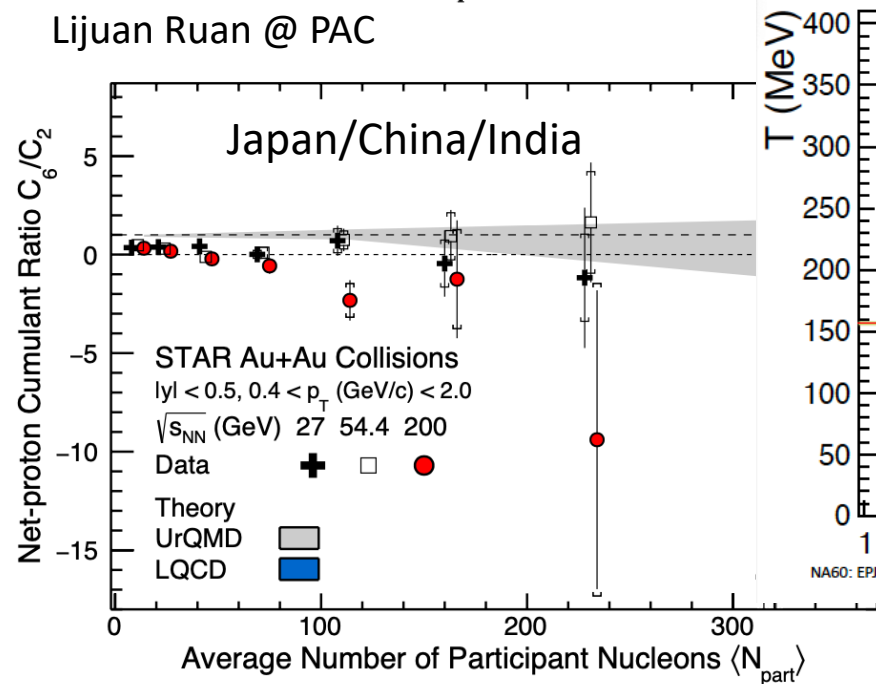
•  $M_0^+$  has the largest intercept so the corresponding process dominates at large  $s$ .

• Rapidity dependence estimated (see Fig. 7)

# Heavy-ion programs less related to EIC



Lijuan Ruan @ PAC



To address important questions about the inner workings of the QGP

- What is the nature of the 3-dimensional initial state at RHIC energies?  $r_n$  over a wide rapidity,  $J/\psi$   $v_1$ , photon Wigner distributions
- What is the precise temperature dependence of shear and bulk viscosity?  $v_n$  as a function of  $\eta$
- What can be learned about confinement from charmonium measurements?  $J/\psi$   $v_2$
- What is the temperature of the medium? Different  $\Upsilon$  states,  $\psi(2S)$ , thermal dileptons
- What are the electrical, magnetic, and chiral properties of the medium?  $\Lambda$ ,  $\Xi$ ,  $\Omega$   $P_H$  and  $K^*$ ,  $\phi$ ,  $J/\psi$   $\rho_{00}$ , thermal dileptons, CME observables
- What are the underlying mechanisms of jet quenching at RHIC energies? What do jet probes tell us about the microscopic structure of the QGP as a function of resolution scale?  $\gamma_{\text{dir}}+\text{jet}$   $I_{AA}$ ,  $\gamma_{\text{dir}}+\text{jet}$  acoplanarity, jet substructure
- What is the precise nature of the transition near  $\mu_B=0$ ? Net-proton  $C_6/C_2$
- What can we learn about the strong interaction? Correlation functions

To inform EIC physics with photon induced processes:

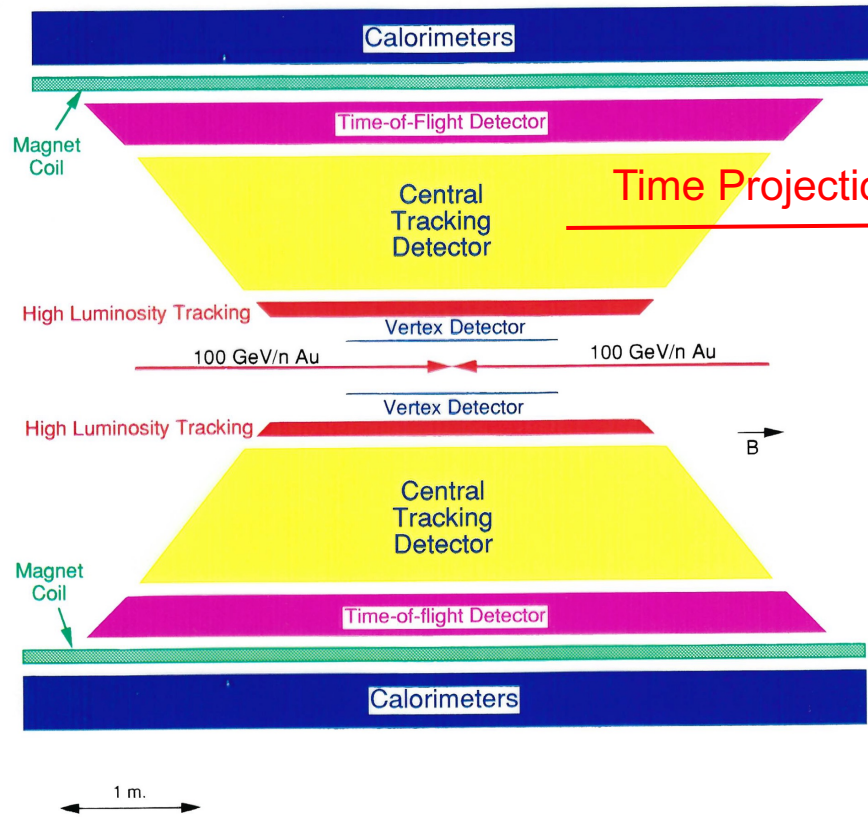
- Probe gluon distribution inside the nucleus: vector mesons ( $J/\psi$ ), dijets (?)
- Search for collectivity and signatures of baryon junction: inclusive charge particles and cross sections,  $v_n$ , identified particle spectra



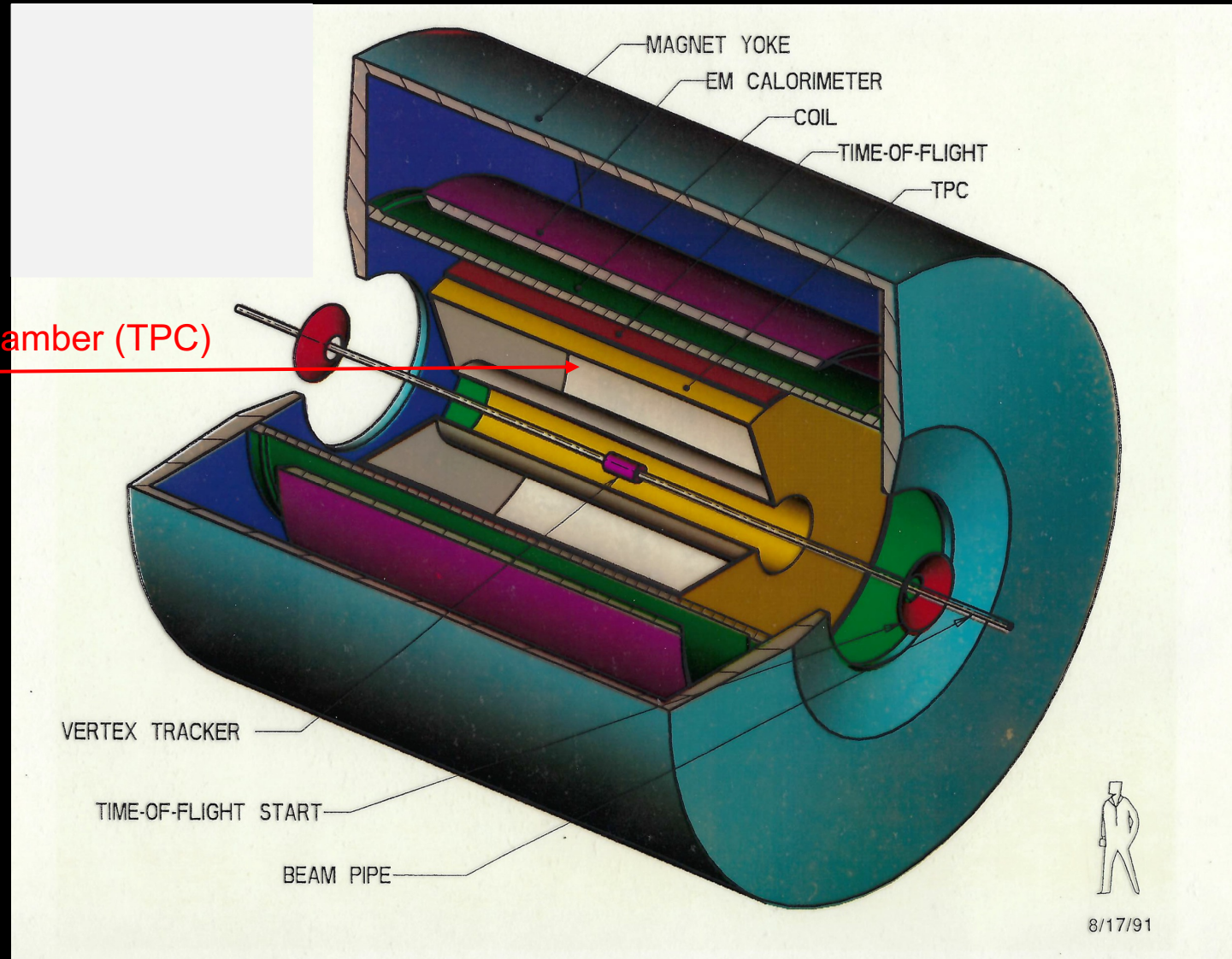
# Design Evolution for Experiment at RHIC

## Conceptual Design for a RHIC Experiment on Particle and Jet Production

UC-Davis, UCLA, U. Frankfurt, Johns Hopkins U., Kent State U., Lawrence Berkeley Lab., Purdue U., Texas A&M U., U. Washington, Zagreb-Boskovic Inst.



J.W. Harris  
6/20/90

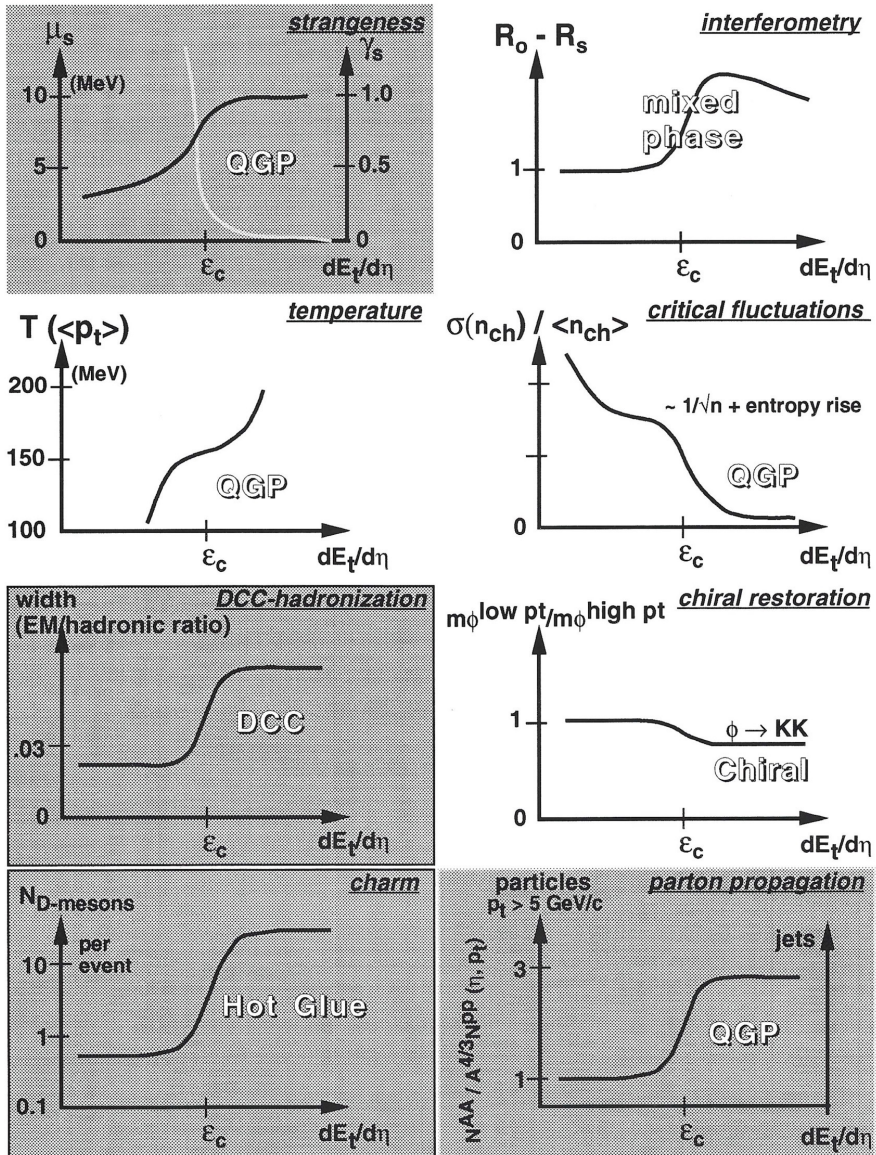


8/17/91

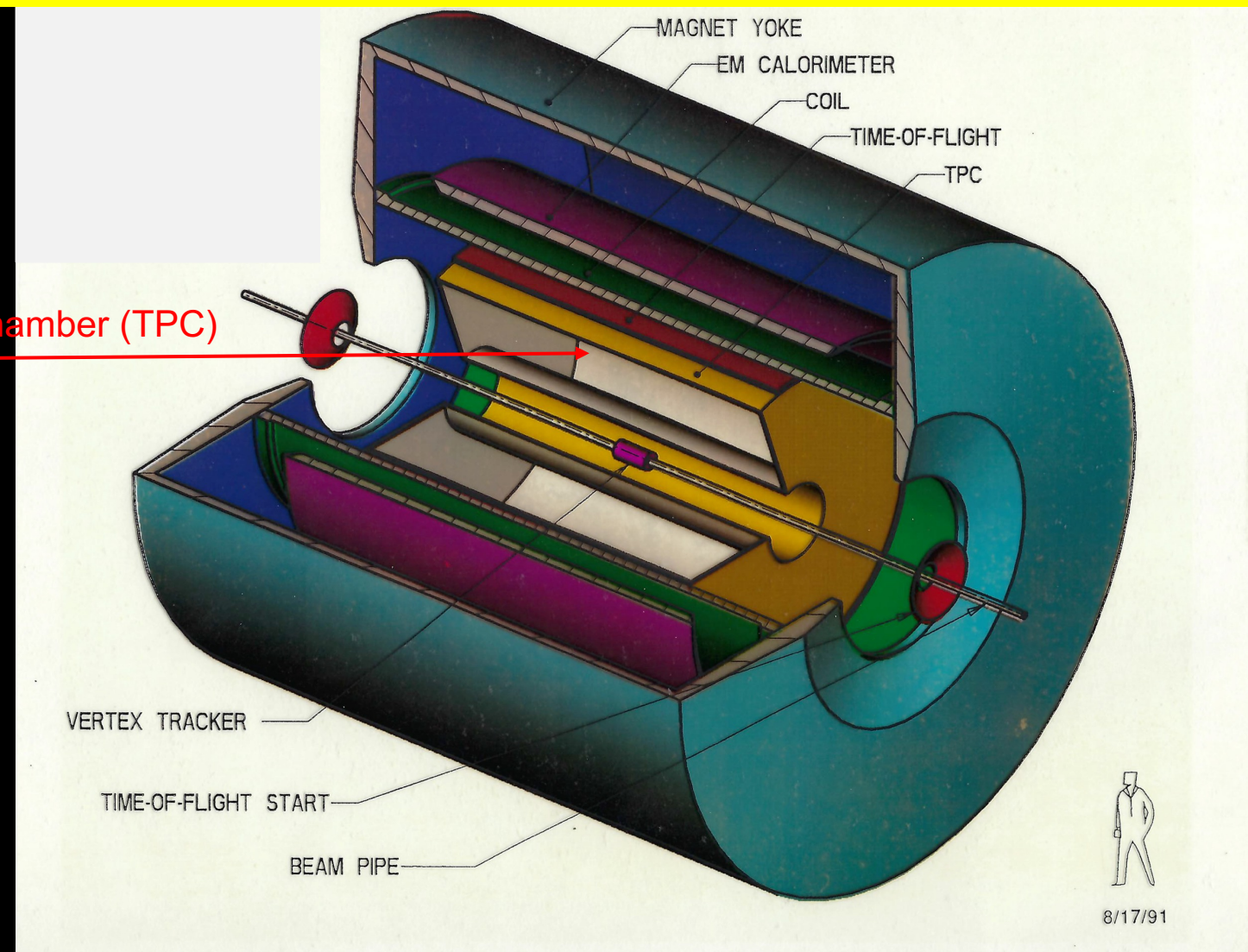


# Design Evolution for Experiment at RHIC

## STAR SIGNATURES



NONE of the signatures came true, but we went on to discover greater things!



8/17/91

☐ STAR Additional Detectors    ☐ STAR Baseline



# STAR physics is well connected to EIC

